

5-2018

An Underwater Vehicle Navigation System Using Acoustic and Inertial Sensors

Khalid M. Alzahrani

Follow this and additional works at: <https://commons.erau.edu/edt>



Part of the [Mechanical Engineering Commons](#)

Scholarly Commons Citation

Alzahrani, Khalid M., "An Underwater Vehicle Navigation System Using Acoustic and Inertial Sensors" (2018). *Dissertations and Theses*. 397.
<https://commons.erau.edu/edt/397>

This Thesis - Open Access is brought to you for free and open access by Scholarly Commons. It has been accepted for inclusion in Dissertations and Theses by an authorized administrator of Scholarly Commons. For more information, please contact commons@erau.edu.

AN UNDERWATER VEHICLE NAVIGATION SYSTEM USING ACOUSTIC AND
INERTIAL SENSORS

by

Khalid M Alzahrani

A Thesis Submitted to the College of Engineering Department of Mechanical
Engineering in Partial Fulfillment of the Requirements for the Degree of
Master of Science in Mechanical Engineering

Embry-Riddle Aeronautical University
Daytona Beach, Florida
May 2018

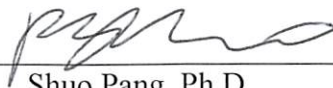
AN UNDERWATER VEHICLE NAVIGATION SYSTEM USING ACOUSTIC AND
INERTIAL SENSORS

by

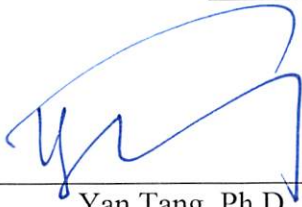
Khalid M Alzahrani

This thesis was prepared under the direction of the candidate's Thesis Committee Chair, Dr. Shuo Pang, Professor, Daytona Beach Campus, and Thesis Committee Members Dr. Yan Tang, Professor, Daytona Beach Campus, and Dr. Darris White, Professor, Daytona Beach Campus, and has been approved by the Thesis Committee. It was submitted to the Department of Mechanical Engineering in partial fulfillment of the requirements for the degree of Master of Science in Mechanical Engineering

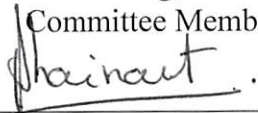
Thesis Review Committee:



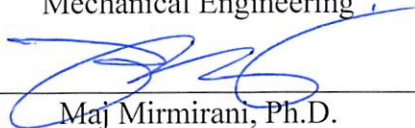
Shuo Pang, Ph.D.
Committee Chair



Yan Tang, Ph.D.
Committee Member



Jean-Michel Dhainaut, Ph.D.
Graduate Program Chair,
Mechanical Engineering



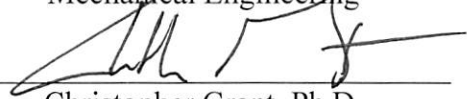
Maj Mirmirani, Ph.D.
Dean, College of Engineering



Darris White, Ph.D.
Committee Member



Eduardo Divo, Ph.D.
Department Chair,
Mechanical Engineering



Christopher Grant, Ph.D.
Associate Vice President of Academics

4/25/18

Date

Acknowledgments

I would like to thank my thesis adviser Dr. Shuo Pang for his guidance and support throughout this research. Furthermore, I would like to thank my committee members, Dr. Yan Tang and Dr. Darris White for taking time for providing feedback and reviewing this thesis. In addition, I am grateful for Dr. Eduardo Divo and Dr. Jean-Michel Dhainaut for their guidance and advice during my master's degree.

I would also like to thank Lingxiao Wang for supporting and helping me to make this research successful.

Moreover, I am very grateful to Albert Obi for all the encouragement, advice, and making me believe in myself. Also, special thanks to Said Hamada and Sakhor Alswat for supporting and advising.

I am extremely grateful to my mother, father, wife, and daughters for their love, prayers, and sacrifices. It would not be completed without their support.

Abstract

Researcher: Khalid M Alzahrani

Title: An Underwater Vehicle Navigation System Using Acoustic and Inertial Sensors

Institution: Embry-Riddle Aeronautical University

Degree: Master of Science in Mechanical Engineering

Year: 2018

Unmanned Underwater Vehicles (UUVs) have become an essential tool for different underwater tasks. Compared with other unmanned systems, the navigation and localization for UUVs are particularly challenging due to the unavailability of Global Positioning System (GPS) signals underwater and the complexity of the unstable environment. Alternative methods such as acoustic positioning systems, Inertial Navigation Systems (INS), and the geophysical navigation approach are used for UUV navigation. Acoustic positioning systems utilize the characteristics of acoustic signals that have a lower absorption rate and a more extended propagation distance than electromagnetic signals underwater. The significant disadvantage of the INS is the “drift,” the unbounded error growth over time in the outputs. This thesis is aimed to study and test a combined UUV navigation system that fuses measurements from the INS, Doppler Velocity Log (DVL), and Short Baseline (SBL) acoustic positioning system to reduce the drift. Two Kalman filters are used to do the fusion: the Extended Kalman Filter (EKF) and the Unscented Kalman Filter (UKF). After conducting the experiments and simulation, the results illustrated the INS/SBL fusion navigation approach was able to reduce the drift problems in the INS. Moreover, UKF showed a better performance than the EKF in the INS.

Table of Contents

Thesis Review Committee	ii
Acknowledgments.....	iii
Abstract.....	iv
Table of Contents.....	v
List of Tables	viii
List of Figures.....	ix
Chapter I.....	1
1 Introduction.....	1
1.1. The significance of the Study	4
1.2. Statement of the Problem.....	5
1.3. Purpose Statement.....	6
1.4. List of Acronyms	7
Chapter II	8
2 Literature Review	8
2.1 AUV Navigation.....	8
2.1.1 Inertial Navigation	9
2.1.2 Geophysical Navigation.....	12
2.1.3 Acoustic Navigation.....	14
2.2 Filtering and Estimation.....	17
Chapter III.....	19
3 Methodology.....	19
3.1 Research Approach.....	19

3.2	The Platform	20
3.3	Reference Frames.....	20
3.4	Onboard sensors.....	21
3.5	Inertial Navigation System	22
3.5.1	Kinematics	23
3.5.2	The transformation between NED and Body Frames	23
3.5.2.1	Linear Velocity Transformation	23
3.5.2.2	Angular Velocity Transformation.....	25
3.5.3	INS errors.....	26
3.6	The External Measurement (SBL).....	27
3.7	Kalman Filter	31
3.7.1	The Kalman filter algorithm	34
3.8	Extended Kalman Filter	35
3.8.1	Extended Kalman Filter algorithm.....	39
3.9	Unscented Kalman Filter	39
3.10	Summary of Three Kalman Filters	43
3.10.1	The error variance Q and R.....	44
3.11	EKF Application for the AUV Navigation	45
3.12	UKF Application for the AUV Navigation.....	47
Chapter IV	49
4	Results.....	49
4.1	The Measurements Error Covariance	49
4.2	The INS and SBL Simulation	53

4.3	The Simulation Results	55
4.4	The Experiments Results	60
4.4.1	INS Path Based on EKF.....	61
4.4.2	INS Path Base on the UKF	68
4.4.3	Compare the Paths from The EKF and UKF	71
4.4.4	INS/SBL Fusion Navigation Approach Based on EKF....	74
	Chapter V	80
5	Discussion and Conclusions	80
5.1	Discussion.....	80
5.1.1	The INS navigation method.....	80
5.1.2	The performance of EKF and UKF	80
5.1.3	INS/SBL navigation approach	81
5.2	Conclusions.....	82
6	References.....	83

List of Tables

		Page
Table		
1.	Table 3.1 Accelerometer and gyro errors sources [22].	26
2.	Table 3.2 The algorithm of the Kalman filter [43].	35
3.	Table 3.3 The EKF process.	38
4.	Table 3.4 The algorithm of the Extended Kalman Filter [43].	39
5.	Table 3.5 The Unscented Kalman Filter's algorithm.	43
6.	Table 3.6 The comparison of the three filters.	43
7.	Table 4.1 The variance of measurements from the inertial sensors.	52
8.	Table 4.2 The true measurements as a sine wave for the simulation.	56
9.	Table 4.3 The initial yaw angles in all tests.	64
10.	Table 4.4 The differences between the measured initial yaw angles and correct initial yaw angles.	65
11.	Table 4.5 Comparison of distances between start points and end points in four tests.	66
12.	Table 4.6 Comparison of the estimated lengths with the swimming pool length.	66
13.	Table 4.7 Comparison of distances between start points and end points in the three tests.	67
14.	Table 4.8 Comparison of the estimated lengths with the swimming pool length.	69
15.	Table 4.9 Comparison of distances between start points and end points in the three tests of Nov 11th tests.	70
16.	Table 4.10 Comparison of UKF and EKF in terms of distances between start points and end points.	72
17.	Table 4.11 Comparison of UKF and EKF in terms of distances between start points and end points.	73

List of Figures

	Page
Figure	
1. Figure 1.1 Remotely Operated Vehicles called BlueROV [7].....	2
2. Figure 1.2 Bluefin-21 AUV [10].....	3
3. Figure 2.1 Layout of AUV navigation classifications with the sensors that used for each method [18].....	8
4. Figure 2.2 The procedures of IMU of integration sensor data. “b” refers to the body-fixed frame.....	10
5. Figure 2.3 underwater acoustic position systems: LBL system (left), SBL system (central), USBL system (right) [30].....	15
6. Figure 3.1 Yellowfinn II underwater vehicle [22].	19
7. Figure 3.2 The Body-fixed frame and NED frame of the Yellowfinn II.	21
8. Figure 3.3 IMU from Vectornav Inc and Figure 3.4 DVL from Vectornav Inc..	22
9. Figure 3.5 The components of the PILOT acoustic positioning system from Desert Star Inc.....	27
10. Figure 3.6 SBL configuration. The transponder is attached to tracking a target [41].....	28
11. Figure 3.7 Geometry of acoustic propagation with the center of the coordinate in the center of transducers [22].....	29
12. Figure 3.8 Kalman filter process.....	34
13. Figure 4.1 The stationary test for Yellowfinn II [22].	50
14. Figure 4.2 The measurements of the stationary test from the inertial sensors.....	51
15. Figure 4.3 The true velocity compares to measured velocity in the X direction. 56	
16. Figure 4.4 The true trajectory as a sine wave, SBL measurements, and the estimated trajectory.....	57
17. Figure 4.5 The estimation errors in the positions.....	58

18.	Figure 4.6 The true trajectory as a circle, SBL measurements and the estimated trajectory.	59
19.	Figure 4.7 The true trajectory shows a straight line, SBL measurements, and the estimated trajectory.....	59
20.	Figure 4.8 The swimming pool of the campus. The red path represents the expected path, and they are the ‘forward and backward’ path and ‘L’ path.....	60
21.	Figure 4.9 All tests’ estimated paths based on EKF and only used INS for the navigation.....	63
22.	Figure 4.10 Four test on Nov 5th after corrected the heading.	65
23.	Figure 4.11 The Nov 11th tests after correcting the heading.....	67
24.	Figure 4.12 The estimated Paths of the seven tests that were created by using UKF.....	68
25.	Figure 4.13 The Nov 5th tests after correcting the heading.....	69
26.	Figure 4.14 The Nov 11th tests after correcting the heading.....	70
27.	Figure 4.15 Comparison of UKF and EKF paths for tests Nov 5th.....	71
28.	Figure 4.16 Comparison of UKF and EKF paths for tests Nov 11th.....	72
29.	Figure 4.17 The locations of three transducers.....	73
30.	Figure 4.18 The paths of tests 1-4 were from the SBL acoustic positioning system in the local reference frame.....	74
31.	Figure 4.19 The paths of tests 5,6, and 7 were from the SBL acoustic positioning system in the local reference frame.	75
32.	Figure 4.20 Test 3 path from INS and SBL after rotation.	77
33.	Figure 4.21 Paths from the SBL, INS and SBL/INS based on EKF.....	78
34.	Figure 4.22 the true trajectory of test 3.....	79

Chapter I

Introduction

It is estimated that the oceans form about 97% percent of the Earth [1]. The oceans constitute one of the most significant resources that humans depend on. However, the oceans are not easy to explore. They are risky, deep, and complex, making it difficult to explore and study. Because of that, only 5-7 percent of oceans have been reviewed or investigated [2]. To better study and explore this vital resource, humans have invented and developed different tools and machines with some of the most recent being Unmanned Underwater Vehicles (UUVs).

Before using or discovering UUVs, researchers use manned underwater vehicles for their exploration. However, due to high operational costs and issues related to operator fatigue and personal safety, the use of manned underwater vehicles is quite limited [3]. Consequently, UUVs have become an essential tool for different underwater tasks because they have higher endurance, speed and depth capability, as well as a higher factor of safety [4]. In 1953, Dimitri Rebikoff developed the first Remotely Operated Vehicle (ROV), which was nicknamed POODLE [5] and was probably the first type of UUV recorded in history. ROVs are a tethered underwater robot that allows the operator to stay on the surface and control the vehicle from a distance while the ROV performs tasks under the water, Figure 1.1 shows an example of an ROV [6]. ROVs have some limitations, such as the physical connection between the ROV and the operator via cables. Moreover, errors are more likely to happen when humans are involved.

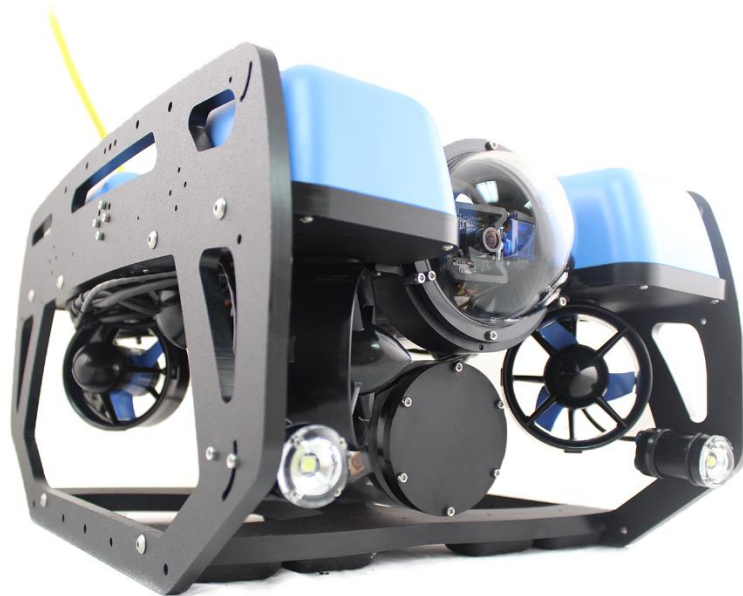


Figure 1.1 Remotely Operated Vehicles called BlueROV [7].

More recent advancements have converted the ROV into an Autonomous Underwater Vehicle (AUV). AUVs are an intelligent type of UUV that operate independently and have no connecting cables [8]. Moreover, AUVs can offer sufficient and more accurate data than ROVs, especially when performing surveys, search and find missions, or seafloor mapping [9]. Since AUVs do not require a human operator to control the vehicle, they can operate for long hours without fatigue, thereby saving time and money. An example of an AUV is the Bluefin robot as shown in Figure 1.2. The General Dynamics Mission Systems owned the Bluefin robot and was developed in an MIT laboratory in conjunction with other laboratories [10]. The Bluefin robot can be used for a wide variety of missions including for defense, commercial, and scientific purposes. One of the well-known uses of Bluefin was in searching for the Malaysia Airline flight 370 in 2014 [11].



Figure 1.2 Bluefin-21 AUV [10].

The purpose of ROVs for underwater research is still widespread with a constant quest for sorting out a more efficient and effective system. Nonetheless, the benefits that ROV's offer including better maneuverability and streaming of near real-time imagery for improved, on-the-spot decision making, have not been surmounted by the AUVs [3]. The more sophisticated autonomous systems rarely match the benefit of always having a human in the loop for online mission changes and implementation. It could imply that, for the foreseeable future, ROVs would remain a very crucial part of ocean researchers. Since ROVs are more affordable than the AUVs in the open market, one concept would be to automate the ROV by incorporation of a navigation system.

UUVs have a wide range of commercial and military applications. Commercially, they use them for ocean surveys and resource assessment, seafloor mapping, geological sampling, detecting oceanographic and geological events, and platform inspection [12]. Other applications include pipeline inspection, oil and gas exploration, underwater structures and environmental remediation among others [12]. The military applications of UUV's are not limited to search and rescue operations, and diver observation, but

other purposes such as intelligence gathering and naval operations. Many of these tasks require precise, careful navigation to be performed successfully. Therefore, most UUVs utilize sophisticated navigation aids and sensors to complete their functions.

This thesis covered and summarized several methods than used for estimating and filtering the AUV position. Consequently, two methods of AUV navigations are studied and tested, and the two navigation methods are the inertial navigation and the acoustic navigation. The measurements from these two methods are fused by using the Extended Kalman Filter (EKF) and the Unscented Kalman Filter (UKF) to get an estimated position of the AUV.

1.1. The significance of the Study

The utilization of UUVs for underwater research is spreading across the world with a constant quest for seeking out more efficient and effective navigation systems. The Global Positioning System (GPS) is one of the most common operations used for navigation today especially for ground and aeronautical vehicles. However, most AUVs cannot utilize GPS for navigation as the signals are unavailable when the vehicle is not on the surface of the water [9]. This means that expensive high-performance sensors must be used to navigate underwater. Small-vehicle ROVs cost \$10,000–\$100,000 each [13]. On the other hand, AUVs are even more expensive than ROVs. For instance, REMUS 600 an AUV, costs the Navy around \$1.3 million each [14]. Lower cost AUVs can start at \$50,000 such as Iver2-580-S, a standard AUV [15]. The high-end sensors used for navigation and localization of the vehicle contribute to the significant portion of the cost. The high price of a UUV is one of the reasons why only 5-7 percent of oceans have been studied or discovered [2].

Regrettably, there is a high correlation between the quality of navigation and the grade of sensors being used with low-grade sensors, which produces large navigation errors while high-end sensors are generally more reliable [16]. Therefore, studying and fusing affordable AUV navigation systems and using a variety of filters, which will present on the purpose statement, could increase the accuracy of localization and contribute on expanding the ability for researchers and scientists to study and discover the underwater life and resources.

1.2. Statement of the Problem

A considerable amount of AUV's applications as demonstrated previously demand precise accuracy on their localization to perform their tasks efficiently. To successfully achieve that, AUVs must have a navigation system to know their location and orientation. However, one major challenge with AUV's navigation that needs to be addressed is the unavailability of the GPS signals under the water. The GPS solutions are impracticable because seawater is impermeable to electromagnetic signals [17]. The GPS is one of the more common navigation systems that widely used for ground and aeronautical vehicle today. Also, sometimes when high accuracy or fast response required, the GPS system is fused with a different kind of a navigation system to get a better result.

Unfortunately, UUVs have the inherent disadvantage of instability about the six degrees of freedom, mainly when operating in the highly complex, unstable, and dynamic environment such as the ocean depths [4]. Inertial navigation and acoustic navigation are most common methods of AUV navigation to navigate under the water. However, each one has its limitations and disadvantages such as acoustic navigation has a limit

bandwidth, low data rate, high latency, varying sound speed due to changing water temperature and saltness, and unreliability [18]. On the other hand, Inertial Navigation System (INS) suffers from drifting over time due to the measurement errors of its inertial sensors. Nevertheless, all of the methods have an error. These attributes the errors to a variety of reasons such as noise and unknown biases [19]. Therefore, all these challenges need to be considered to successfully navigate and keep the AUV in the desired location and orientation all the time.

1.3. Purpose Statement

The fact that when AUV navigation relies only on one navigation system, high grade and expensive sensors are needed to navigate. However, even with that, measurement error is expected to happen, but it will be less than when low-cost sensors are used alone. Consequently, when combining two or more different AUV navigation methods, that increase the performance and yield to obtain an optimal estimate of AUV position [18].

This thesis aimed to study and test a combined AUV navigation system that fuses measurements from the Inertial Measurements Unit (IMU), Doppler Velocity Log (DVL), and Short Baseline (SBL) acoustic positioning system. The fusion is carried out by using two different Kalman filters, the Extended Kalman Filter (EKF) and the Unscented Kalman Filter (UKF), to study and evaluate each kind. In addition, experiments and simulation are used to compare accuracy and performance of this algorithm that tests under myriads of scenarios and to assess its performance.

1.4. List of Acronyms

UUV	Unmanned Underwater Vehicle
AUV	Autonomous Underwater Vehicle
ROV	Remotely Operated Vehicle
GPS	Global Positioning System
INS	Inertial Navigation System
IMU	Inertial Measurements Unit
DVL	Doppler Velocity Log
DR	Dead-Reckoning
SBL	Short Baseline
KF	Kalman Filter
EKF	Extended Kalman Filter
UKF	Unscented Kalman Filter
SLAM	Simultaneous Localization and Mapping
VAN	Visually Augmented Navigation
SBL	Short Baseline
LBL	Long Baseline
USBL	Ultra-Short Baseline
MEMS	MicroElectroMechanical System
NED	North East Down Frame
DCM	Direction Cosine Matrix
GAS	Globally Asymptotically Stable
DOF	Degree of Freedom

Chapter II

Literature Review

2.1 AUV Navigation

Stutters, Liu, Tiltman, and Brown [9] investigated the different methods used in AUV's navigation. They also show the limitations of each method and compare their suitability when used in different environments. Currently, there are three different standard methods used for the AUV navigation: geophysical navigation, acoustic navigation, and inertial navigation.

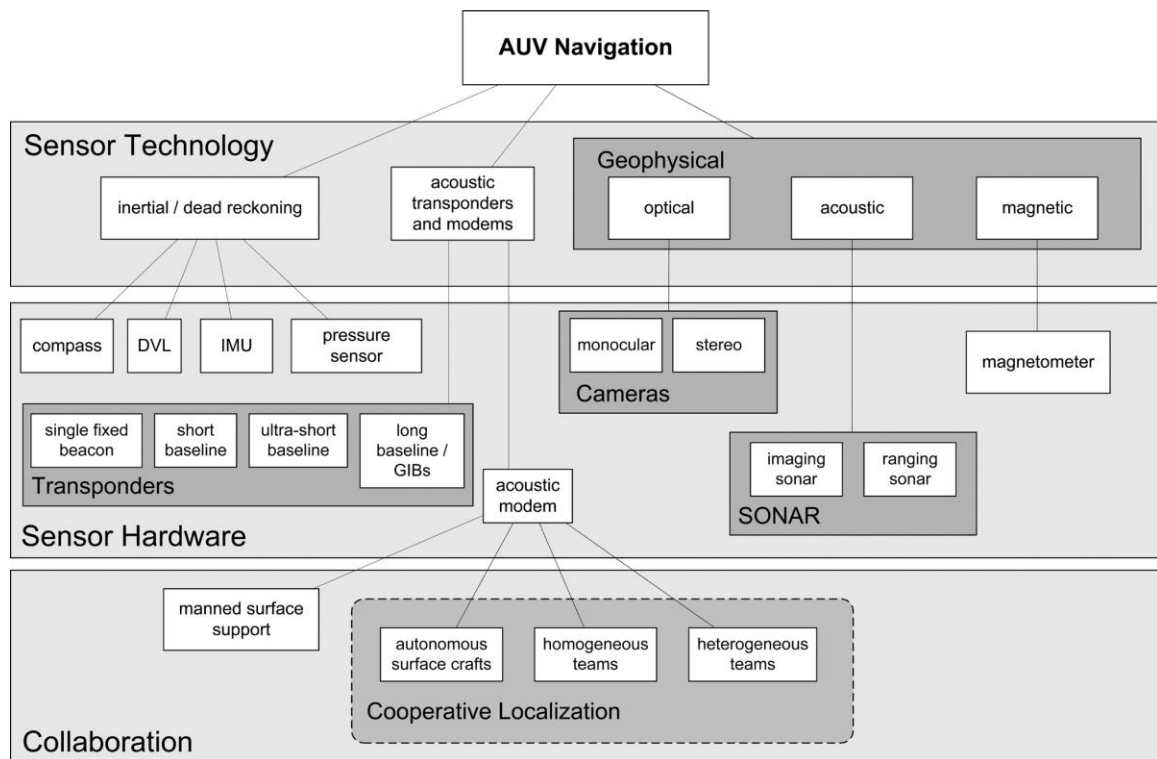


Figure 2.1 Layout of AUV navigation classifications with the sensors that used for each method [18].

2.1.1 Inertial Navigation

Inertial Navigation System (INS) is one of the approaches used to navigate AUV underwater. INS is a relative positioning system that calculates position based on the previous positions [20]. Also, the process of knowing the vehicle's current position by using a previously determined position is called the dead reckoning (DR) [21]. The INS is an enhanced concept of the DR navigation, which includes a computer that can apply digital filter algorithms to improve sensor accuracies. In INS navigation approach, the vehicle is given an initial position before starting the navigation, and then measurements from inertial sensors such as an Inertial Measurement Unit (IMU) or a Doppler Velocity Log (DVL) is used to calculate the vehicle's position [22]. The IMU has three-axes rate gyroscopes, accelerometers, and magnetometers. Cheaper INS can be used for inexpensive AUVs, while the high-performance INS with fiber-optic gyroscopes are limited to more expensive AUVs [9]. Nowadays with the developing on MicroElectroMechanical Systems (MEMS), it becomes possible to manufacture smaller and lighter IMU.

The role of the inertial sensors is to detect and measure motions based on the physical laws of nature. The position of a vehicle can be determined by integrating the measured accelerations, and to obtain the attitude by integrating the measured angular rates [23]. Therefore, the INS can estimate the positions without help from the GPS or any external measurements since the positions are calculated based on onboard sensors' measurements [22]. This makes INS commonly implemented for AUV navigation.

There are two main stages of the traditional INS algorithm. First, the three-axes, measured accelerations from accelerometers are transferred from the body-fixed frame to

the north east down frame (NED), and this happens by multiplying the transposed form of the direction cosine matrix (DCM). The attitude angles which are roll (ϕ), pitch (θ), and yaw (ψ) are calculated from integrating measured angular rates from gyroscope measurements in kinematics equations. Second, the acceleration measurements in the NED frame are integrated to get velocities and then integrated again to get the positions. Figure 2.2 illustrates these procedures of a traditional INS navigation approach.

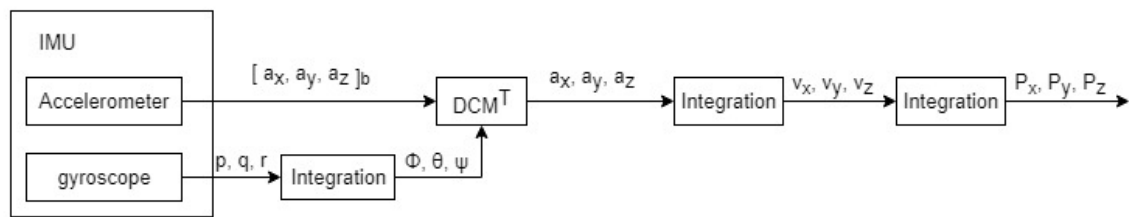


Figure 2.2 The procedures of IMU of integration sensor data. “b” refers to the body-fixed frame.

INS also have disadvantages. The accelerometers built into the system are subject to drift over time. This implies that where AUVs use INS-only navigation systems, there is a gradual accumulation of position error over time. The cause of this error is the difference in the integration of the acceleration and gyro outputs to obtain vehicle position and orientation. This results in the sensor biases, misalignment and temperature variations present in the system [24]. Also, the uncertainties in measurements can be caused by external forces such as sea tides, water currents, and winds that can easily shift the AUV positions and affect the INS’s performance. Adding, these unexpected external influences are difficult to measure or estimate by inertial sensors in such a short time.

However, for a short-range navigation mission like in a pool, the performance of the INS alone will be acceptable whereas the drift will not be that significant. Nevertheless, the error or the drift in AUV position for an extended mission will be enormous and unacceptable.

To reduce the drift error especially in long missions, Stutter [9] opined that a sonar Doppler velocity log (DVL) could be used to measure the speed of the sea floor relative to the AUV. Thus, integrating DVL measurement with INS would reduce the vehicle drift over time. Nevertheless, it is pertinent to point out that DVL sonars also have a limited range and require the vehicle to be close to the sea floor to be very useful [9].

Using high-grade sensors is another solution to reduce the drift error. In Panish and Taylor's project [25], they used a laser gyroscope, an optical gyroscope, and a high-quality DVL with inertial sensors to minimize the drift problem in the INS. As shown in the results of their experiments proved that using a high grade of IMU limited the drift and provided excellent performance for the AUV's navigation [25].

In Kennedy's project [3], a flow meter was used instead of DVL to measure the surge velocity. Flow meters have two advantages over DVL. They are less expensive than DVL and do not need to be near the seafloor to measure the velocity [3]. In more shallow waters or operations close to the surface, GPS signal can be integrated with an IMU to obtain estimates of vehicle position and velocity in 6 DOF. In this case, reducing the INS drift can be carried out by fusing the GPS and INS in a state observer [24]. However, this is impracticable in deep sea operations due to limitations of satellite-based navigation systems.

One of the challenges that face INS is to know the initial position of the vehicle before performing the navigation. The reason behind that is the INS only estimate how far the vehicle is traveled but not where the vehicle is, so the knowledge of the initial position is essential. Moreover, if the initial position has an uncertainty, which means the given initial position is not equal to the actual initial position of the vehicle, this uncertainty will propagate in the process of integrations. Also, it will be worse if the initial position is unknown and in this case, the INS will not navigate for the AUV [22].

The uncertainty on the initial position can be solved by using external measurements to assist the INS with an initial position of the vehicle. This method was implemented by a team from Massachusetts Institute of Technology (MIT) [26]; they used Cooperative Navigation Aids (CNAs) method to solve the drift and the initial position problems in the INS. The CNA system is a merged system of an autonomous surface craft and an AUV. The craft is equipped with an acoustic modem, a GPS module, and a compass sensor. Therefore, the positions and attitudes can be determined from these external sensors. The craft transmitted these external measurements to the AUV, and these measurements were used to correct INS's errors and produce the accurate information for the AUV navigation [26].

2.1.2 Geophysical Navigation

Geophysical navigation is a form of navigation where physical features of the operating environment are used to produce an estimate of the AUV's location. To achieve this, a sonar sensor, an optical sensor or magnetometer are used. The system depends on the sensor data that is used for detecting, identifying and classifying some environmental features. However, due to the low resolution of the sensors and the unstructured shape of

natural features, it is difficult to extract features from the sensor data [9]. To mitigate this challenge, underwater cameras are used as more reliable sensors. Nonetheless, these are also restricted in their effective range. Thus, any vehicle utilizing this method might need to operate very close to the ocean bed or object of interest [9].

The two kinds of the underwater map that can use as references for geophysical data are bathymetric sonar and magnetic field maps. Therefore, AUVs can use these existing maps of the area to navigate or if the map is not available, AUV can constructing such a map over the mission that helps to navigate around the area [9]. Positions of external features are fixed and known. Therefore, when a vehicle detects and identifies one of these features, it can utilize the identified feature's position as a reference point to correct its navigation's errors.

Many technics use the geophysical method to navigate, and one of these technics is Simultaneous Localization and Mapping (SLAM). SLAM is a process by which a robot can autonomously build a map of its environment and at the same time use this map to localize and navigate itself within its environment [27]. The SLAM method consists of two primary procedures: mapping and sensing. The mapping procedure is the generation of an estimated local map by extracting landmarks from the environment, and the sensing procedure is an estimation of the robot's positioning in the generated map based on these landmarks' locations as references to perform the navigation.

SLAM methodology can be classified as feature-based, where features are extracted and kept in the space, or view-based, where poses corresponding to measurements are kept in the state space. In the feature-based SLAM, features are extracted from sensors' measurements, and the state space model is updated at each time

when sensors observe new features [27]. In Salvi, Petillot and Batlle article [28], a local 3D map of the seabed structure was built by using a stereo camera attached to the AUV. The locations of the detected seabed landmarks were utilized as reference points to improve the navigation accuracy of AUV by removing INS's drift that happens over time. In view-based SLAM, at each pose, the image of the environment is comparing with the previous image. In Eustice paper, the visually augmented navigation (VAN) was used to improve the navigation accuracy based on vision-based SLAM. It employed a camera to capture seafloor imageries, and based on changing between two imageries generates camera measurements to measure velocities and attitude of the AUV [29].

In Eustice and Salvi papers [27, 28], both of them use extended Kalman filters (EKF) to fuse the sensors measurements to get a better estimation of the position. In both view-based SLAM and feature-based SLAM, the EKF is implemented to linearize the system model using the Taylor expansion. The SLAM is applicable for both 2D and 3D motions. For the AUV navigation, the 3D motions SLAM is more suitable and closer than a 2D motion to a realistic navigation phenomenon.

2.1.3 Acoustic Navigation

Since the GPS is an external positioning system but does not penetrate below the sea surface, other external positioning systems can operate underwater such as acoustic positioning system. Acoustic navigation employs some form of acoustic transponder beacons which allow the AUV to determine its position [30]. The estimated AUV position is relative to the local reference frame and can be calculated from the ranges between each transducer and the transponder. The acoustic positioning system utilizes acoustic signals since they have a lower absorption rate in the water as compared with

electromagnetic signals that GPS signals use. Consequently, acoustic signals can travel a longer distance in the water than electromagnetic signals, which make acoustic signals suitable for AUV navigation and localization underwater.

The most common methods for AUV acoustic positioning system are Long Baseline (LBL) that uses at least two widely separated beacons placed on the seafloor [30]. The other Short Baseline (SBL) uses three beacons that are placed separately at the end of a vessel hull, and Ultra-Short Baseline (USBL) that are closely placed together on a single surface vessel [9]. The word ‘baseline’ refers to an imaginary line that connects two beacons. USBL systems are identical to SBL concepts excluding that the transducers at USBL system are compiled into a single transceiver assembly or an array of transducer elements in a single transceiver [30]. Figure 2.3 illustrates the difference between the three kinds of the acoustic positioning systems. The majority of acoustic positioning systems have at least three transducers and one transponder.

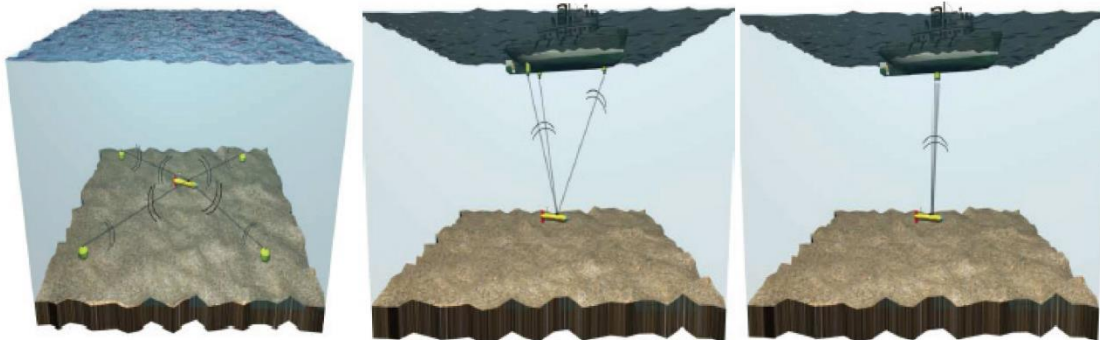


Figure 2.3 underwater acoustic position systems: LBL system (left), SBL system (central), USBL system (right) [30].

In the three types, the transponder is attached to the AUV, and transducers are placed differently, depending on the type of system in operation. Also, since the locations

of transducers are known, a local reference frame can create and select the location of the original point and directions of the horizontal axis and the vertical axis in this local reference frame. Therefore, with knowledge of the beacon positions, the time of flight of the signal, and the local sound speed, the AUV can conclude its location from the intersection of the AUV's probable positions relative to each beacon [9].

The main differences between these three methods are the length of the baseline and locations of transducers. The locations of these methods are discussed previously, and Figure 2.3 shows the differences. Regarding the length of baseline, the USBL system has the shortest baseline that is less than 10 centimeters, while LBL system has the most extended baseline that is in the range from 100 meters to 6000 meters. In the SBL, the baseline's length is from 20 meters to 50 meters, which is suitable to attach to the bottom of ship's hull [31].

Each kind of acoustic positioning systems suits for different missions. For example, an SBL positioning system is proper for a short-range navigation and tracking mission, and an LBL positioning system uses for a long-range mission. One of the typical advantages of all these acoustic positioning methods is that all their approaches can provide the absolute positioning information of the underwater vehicle, which is not practicable for other procedures such as the INS method. This advantage makes the acoustic positioning system act similar to the GPS but under the surface of the water.

Acoustic positioning systems have been used widely for AUV navigation in scientific marine surveys and other missions. In 2008, an experimental research group used an LBL acoustic positioning system to provide AUV positions for an under-ice operation. In their survey of the ocean bottom, they used two spaced stationary beacons

were placed on the seafloor for the LBL acoustic positioning system and multiple beacons that attach to a ship. Therefore, AUV's position is calculated by measuring the sound round-trip traveling periods from the AUV to each beacon to get the distances from the AUV to each beacon.

Combining the acoustic positioning method with the other AUV navigation methods, such as INS method, can improve the accuracy of AUV navigation. For instance, in Ridao project [32], a USBL system was merged with INS to reduce the errors. The USBL provides an absolute position that can use to minimize the drift errors that usually occur on the INS. Also, an information filter was utilized to fuse USBL data and INS data to perform a better navigational performance [32].

However, research shows that there are some disadvantages of using acoustic navigation. In LBL approach, the systems have to be deployed for extended periods of time which increase the costs for deployment and comprehensive calibration at each implementation. On the other hand, Short Baseline (SBL) utilizes a technique where the system is installed on a ship. This significantly increases the signal-to-noise ratio and degrades the accuracy of the acoustic positioning the SBL, Ultra Short Baseline USBL and Long & Ultra Short Baseline (LUSBL) are only accurate in calm weather where there is no ship motion [30].

2.2 Filtering and Estimation

Most of the currently AUVs are installed with multiple sensors that are used to improve the estimation of the vehicle. Each sensor provides the system with a data that needs to fuse with other sensors data throughout a mission to get an optimal estimation of the vehicle's position. This process is called filtering, which is a vital process to

successfully fuse the sensors measurements to obtain an estimate of an AUV position.

Paull, Saeedi, Seto, and Li [18], investigate the different methods of the state estimators that use in an AUV's navigation.

In Yun's paper [33], they used a 12-state complementary filter to fuse data from different sensors including a GPS module, an IMU, a compass, a water speed sensor and a water pressure sensor. Their results from simulations provided a practical approach for tuning filter gains. Also, they used a ground vehicle to verify the overall functioning of the suggested complimentary filter and show an encouraging degree of accuracy [33].

In Wang project, he compared between the extended Kalman filter (EKF) and the Unscented Kalman filter (UKF) for his project. He found that using an unscented Kalman filter for state estimation instead of an extended Kalman filter is more accurate and this would reduce the error [34]. This because underwater vehicles exhibit high nonlinearity in their models, the regular EKF, will not work well in this situation. Adding, the performance of the unscented Kalman filter over the extended Kalman filter has been reported in several publications [35] and [36].

Moreover, Rigby, Pizarro, and Williams [37] used a multi-sensor data fusion method to combine the measurements data from a USBL, a DVL, and a gyro. Instead of using EKF or UKF, they designed a filtering algorithm named as the Globally Asymptotically Stable (GAS) to fuse non-linear measurements from these sensors. Simulation results from their project showed that the GAS filter was able to achieve the same level of performance of the EKF [37].

Chapter III

Methodology

3.1 Research Approach

In this chapter, the INS algorithm and SBL acoustic positioning system are studied. For the estimation and filtering, the Kalman filter is analyzed including the EKF and UKF. A nine-state EKF and UKF algorithms were developed to fuse the inertial sensor measurements and external measurements to perform the AUV navigation successfully. By using a platform, this algorithm was tested in different scenarios, and its behavior was evaluated. The synchronizing approach for different sensors updating rate was also discussed in this thesis. Finally, the simulation also was conducted to verify the performance of navigation system of AUV, the extended Kalman filter (EKF) and to compare the simulation output and eventually the experimental data.

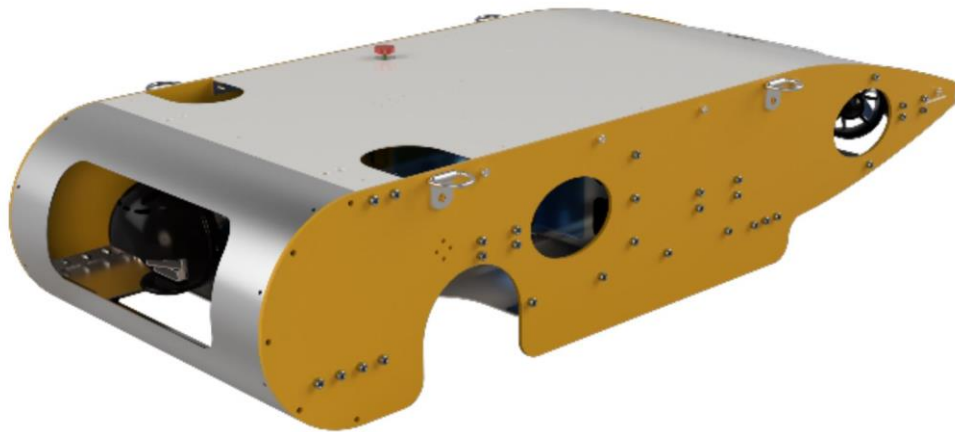


Figure 3.1 Yellowfin II underwater vehicle [22].

3.2 The Platform

To comprehend this research, the platform to be used is the Yellowfinn II underwater vehicle as shown in Figure 3.1. This vehicle was designed and built by the Robotics Association at Embry-Riddle Aeronautical University for the RoboSub underwater robot competition [38]. The proposed navigation approach in this paper was applied on Yellowfinn II for the competition. Seven thrusters from Blue Robotics Inc model T-200 are used to move the AUV on the six degrees of freedom (6-DOF).

3.3 Reference Frames

Two reference frames are presented, which are the body-fixed frame and the North-East-Down (NED) frame. The body-fixed frame with its origin o_b equivalent with the AUV's center of mass and the three axes in the AUV's surge, sway and heave directions [34]. The body-fixed frame does not provide the position of the vehicle because the body-fixed frame is fixed with the AUV. However, the orientation in the body-fixed frame changes with the AUV orientations. Figure 3.2 demonstrates the two reference frames. As shown in this figure, in the body-fixed frame, the X-axis aligns with the longitudinal direction, and the Y-axis aligns with the transversal direction. The Z-axis aligns with the normal axis. The linear velocities along these three axes are stated surge, sway, and heave correspondingly, and the angular rates on the X, Y, and Z axis are Roll rate, Pitch rate, and Yaw rate respectively.

The NED frame is relative to the Earth's reference ellipsoid with the origin o_n [24]. For this frame, the X-axis points to the true North, the Y-axis points to the East, and the Z-axis points to the normal of the Earth's surface. Roll, pitch, and yaw angles are the

orientation that describes the relation from the NED frame to the body-fixed frame. With these angles, we can transfer any parameters in one frame to the other frame. Therefore our goal is to track the position of the AUV in the NED frame.

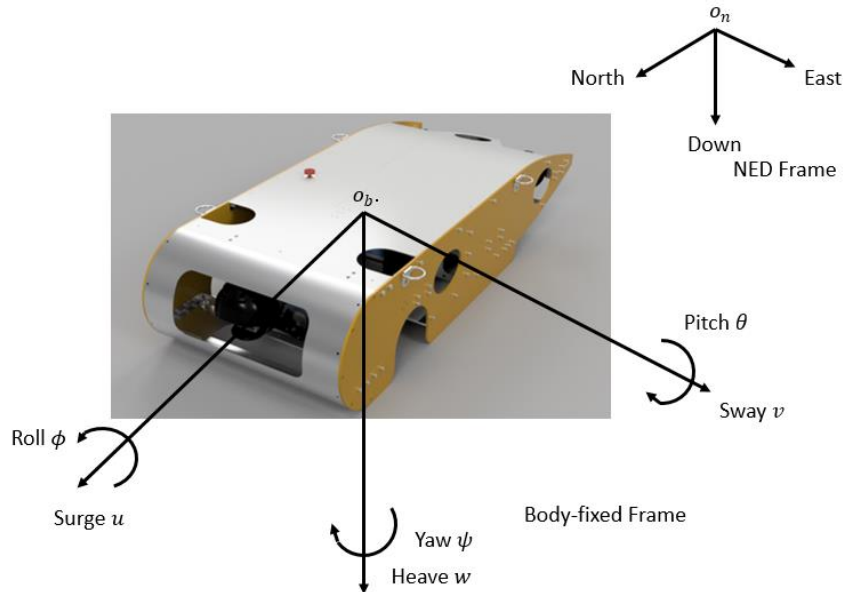


Figure 3.2 The Body-fixed frame and NED frame of the Yellowfin II.

3.4 Onboard sensors

Two sensors are onboard and used for the AUV navigation system, which are IMU and DVL as shown in Figures 3.3 and 3.4, and both of them are from the Vectornav Inc. This particular IMU has an embedded EKF that can calculate the estimated attitude angles. The DVL measures the velocities of the vehicle. All the measurements from the inertial sensors are in the body-fixed frame. Thus, these measurements have to be transferred into the North East Down (NED) frame to perform the navigation.



Figure 3.3 IMU from Vectornav Inc.



Figure 3.4 DVL from Vectornav Inc.

There are 26 measurements recorded from INS. DVL Measurements are V_x , V_y , and V_z , which are the velocities of the AUV, with the unit of a meter per second (m/s). Also, this sensor is embedded with a pressure sensor which the measured water pressure can be converted into the depth of the AUV. IMU with the embedded EKF provided the system with the attitude angles and angular rates calculated from the IMU's are represented as *Roll*, *Pitch*, and *Yaw* in the log. All attitude angles are in the unit of radiant (rad). *Roll rate*, *Pitch rate*, and *Yaw rate* are the angular rates, and they are in the unit of radiant per second (rad/s). Also, this IMU provides the uncertainties in measurements of angular rates, which are useful for the EKF's estimations.

3.5 Inertial Navigation System

Inertial Navigation System (INS) is a relative positioning system that calculates position based on the previous positions [20]. The accelerometers and gyroscopes used to provide the position and the orientation of the AUV. These positions and orientations from the INS are related to an identified initial point, orientation, and velocity [39]. The inertial navigation is based on the application of Newton's laws of motion [40].

3.5.1 Kinematics

As shown in Figure 3.2, the motion of an AUV is in six degrees of freedom, and it describes as the following vectors [24].

$$\boldsymbol{\eta}_1 = \begin{bmatrix} X \\ Y \\ Z \end{bmatrix} \quad \text{the position vector in the NED frame.}$$

$$\dot{\boldsymbol{\eta}}_1 = \begin{bmatrix} V_x \\ V_y \\ V_z \end{bmatrix} \quad \text{the velocities vector in the NED frame.}$$

$$\boldsymbol{\eta}_2 = \begin{bmatrix} \phi \\ \theta \\ \psi \end{bmatrix} \quad \text{Euler angles between the NED frame and the body-fixed frame.}$$

$$\mathbf{v} = \begin{bmatrix} u \\ v \\ w \end{bmatrix} \quad \text{the linear velocities vector in the body-fixed frame.}$$

$$\boldsymbol{\omega} = \begin{bmatrix} p \\ q \\ r \end{bmatrix} \quad \text{the angular velocities vector in the body-fixed frame.}$$

$$\mathbf{a} = \begin{bmatrix} a_x \\ a_y \\ a_z \end{bmatrix} \quad \text{the accelerations vector in the body-fixed frame.}$$

3.5.2 The transformation between NED and Body Frames

The transformation matrices are used to transfer the states between the NED frame and the body-fixed frame.

3.5.2.1 Linear Velocity Transformation

The velocities and accelerations in body-fixed are expressed as posted by Fossen [24]:

$$\mathbf{v} = \mathbf{R}(\boldsymbol{\eta}_2) * \dot{\boldsymbol{\eta}}_1 \quad (3.1)$$

$$\mathbf{a} = \mathbf{R}(\boldsymbol{\eta}_2) * \ddot{\boldsymbol{\eta}}_1 \quad (3.2)$$

Where $\mathbf{R}(\boldsymbol{\eta}_2)$ is the Euler angle rotation matrix with the argument $\boldsymbol{\eta}_2 = [\phi, \theta, \psi]^T$ and is defined as:

$$\mathbf{R}(\boldsymbol{\eta}_2) = \begin{bmatrix} c(\psi)c(\theta) & s(\psi)c(\theta) & -s(\theta) \\ -s(\psi)c(\phi) + c(\psi)s(\theta)s(\phi) & c(\psi)c(\phi) + s(\psi)s(\theta)s(\phi) & c(\theta)s(\phi) \\ s(\psi)s(\phi) + c(\psi)s(\theta)c(\phi) & -c(\psi)s(\phi) + s(\psi)s(\theta)c(\phi) & c(\theta)c(\phi) \end{bmatrix}. \quad (3.3)$$

Where $s(\cdot) = \sin(\cdot)$ and $c(\cdot) = \cos(\cdot)$.

Since The $\mathbf{R}(\boldsymbol{\eta}_2)$ is an orthogonal matrix, the transpose form of $\mathbf{R}(\boldsymbol{\eta}_2)$ is equal to the inverse form.

$$\mathbf{R}(\boldsymbol{\eta}_2)^{-1} = \mathbf{R}(\boldsymbol{\eta}_2)^T \quad (3.4)$$

Therefore, velocities and accelerations can be transferred from the body-fixed frame to the NED frame by these equations:

$$\boldsymbol{\eta}_1 = \mathbf{R}(\boldsymbol{\eta}_2)^T * \mathbf{v} \quad (3.5)$$

$$\dot{\boldsymbol{\eta}}_1 = \mathbf{R}(\boldsymbol{\eta}_2)^T * \mathbf{a} \quad (3.6)$$

The velocities $\boldsymbol{\eta}_1 = [V_x, V_y, V_z]^T$ can be obtained by integrating the accelerations $\dot{\boldsymbol{\eta}}_1$. For the discrete time system, these integrations can be stated as:

$$V_{x_k} = V_{x_{k-1}} + a_{x_{k-1}} * dt \quad (3.7)$$

$$V_{y_k} = V_{y_{k-1}} + a_{y_{k-1}} * dt \quad (3.8)$$

$$V_{z_k} = V_{z_{k-1}} + a_{z_{k-1}} * dt \quad (3.9)$$

For the continuous time system, these integrations are:

$$V_x = V_{x0} + \int a_x * dt \quad (3.10)$$

$$V_y = V_{y0} + \int a_y * dt \quad (3.11)$$

$$V_z = V_{z0} + \int a_z * dt \quad (3.12)$$

where V_{x0} , V_{y0} , and V_{z0} are initial velocities.

After two integrations of the accelerations, we can obtain the position vector of the AUV

$\boldsymbol{\eta}_1 = [X, Y, Z]^T$ in the NED frame are:

$$X_k = X_{k-1} + V_{x_{k-1}} dt \quad (3.13)$$

$$Y_k = Y_{k-1} + V_{y_{k-1}} dt \quad (3.14)$$

$$Z_k = Z_{k-1} + V_{z_{k-1}} dt \quad (3.15)$$

For the continuous time system:

$$X = X_0 + \int V_x dt \quad (3.16)$$

$$Y = Y_0 + \int V_y dt \quad (3.17)$$

$$Z = Z_0 + \int V_z dt \quad (3.18)$$

where X_0 , Y_0 , and Z_0 are the initial positions in the NED frame.

3.5.2.2 Angular Velocity Transformation

The angular velocities for roll, pitch, and yaw can be obtained by transferring the angular rates in the body-fixed frame through the transformation matrix:

$$\boldsymbol{\eta}_2 = T(\boldsymbol{\eta}_2) \boldsymbol{\omega} \quad (3.19)$$

where:

$$T(\boldsymbol{\eta}_2) = \begin{bmatrix} 1 & \sin\phi \tan\theta & \cos\phi \tan\theta \\ 0 & \cos\phi & -\sin\phi \\ 0 & \sin\phi/\cos\theta & \cos\phi/\cos\theta \end{bmatrix}. \quad (3.20)$$

Next, expanding and integrating equation 3.19 yield the Euler angles $\boldsymbol{\eta}_2 = [\phi, \theta, \psi]^T$. For

the discrete time these angles can be expressed in following equations:

$$\phi_k = \phi_{k-1} + (p_{k-1} + \sin\phi_{k-1} \tan\theta_{k-1} q_{k-1} + \cos\phi_{k-1} \tan\theta_{k-1} r_{k-1}) dt \quad (3.21)$$

$$\theta_k = \theta_{k-1} + (\cos\phi_{k-1} q_{k-1} - \sin\phi_{k-1} r_{k-1}) dt \quad (3.22)$$

$$\psi_k = \psi_{k-1} + (q_{k-1} \sin\phi_{k-1}/\cos\theta_{k-1} + r_{k-1} \cos\phi_{k-1}/\cos\theta_{k-1}) dt \quad (3.23)$$

For continuous time system, these integrations can be expressed in following equations:

$$\phi = \phi_0 + \int (p + q \sin\phi \tan\theta + r \cos\phi \tan\theta) dt \quad (3.24)$$

$$\theta = \theta_0 + \int (q \cos\phi - r \sin\phi) dt \quad (3.25)$$

$$\psi = \psi_0 + \int (q \sin\phi/\cos\theta + r \cos\phi/\cos\theta) dt \quad (3.26)$$

where ϕ_0 , θ_0 , and ψ_0 are the initial angles.

In Yellowfin II, all integrations are done in the discrete time. This is because integration of the discrete time is efficiently processed with digital computers than continuous time integration.

3.5.3 INS errors

Table 3.1 details the sources of errors in the INS. These errors are usually described by uncertainties of the inertial sensors. Errors associated with accelerometers are as follows: accelerometer measurement noises, biases in measurement, scaling errors, alignment errors, and nonlinearity of the accelerometer. When these errors are being corrected via calibration of the accelerometer, the errors are described as accelerometer scale factors. With the gyro, there can be errors. Such errors include measurement noises, drift, scale factor, and alignment of the Gyro.

Table 3.1 Accelerometer and gyro errors sources [22].

Accelerometer Errors	Gyro Errors
Accelerometer measurement noise: random error added to the measurement	Gyro measurement noise: random additive error on the measurement
Accelerometer bias: bias in the measured specific force	Gyro drift (bias): bias in the measured angular rate
Accelerometer alignment: error in the alignment of the accelerometer measurement axes from the platform axes	Gyro alignment: error in the alignment of the gyro measurement axes from the orthogonal platform axes
Accelerometer nonlinearity: deviation from the desired linear input/output relationship	Gyro g sensitivity: the sensitivity of the gyro output to force applied along or perpendicular to the sensitive axis of the gyro

In scenarios where we do not have external measurements to eliminate the drift in the INS, the gyro and accelerometer errors are factored into the outputs of the INS. In an

ideal situation where the initial estimation, IMU measurements, integrations calculations, are perfect and the navigation task meant to be done for a short period, we can have full confidence on the INS excluding other external aids or filters. However, this is not always the case. There can be errors in the initial values or IMU measurements. Hence, we are limited to a few rounds before the errors in the velocity and position become too large and influence the results significantly.

Owing to scenarios like these, there is a need for external measurement tools to correct errors in the INS and fuse the IMU with the external sensors. This will help in the estimation of the position vector.

3.6 The External Measurement (SBL)

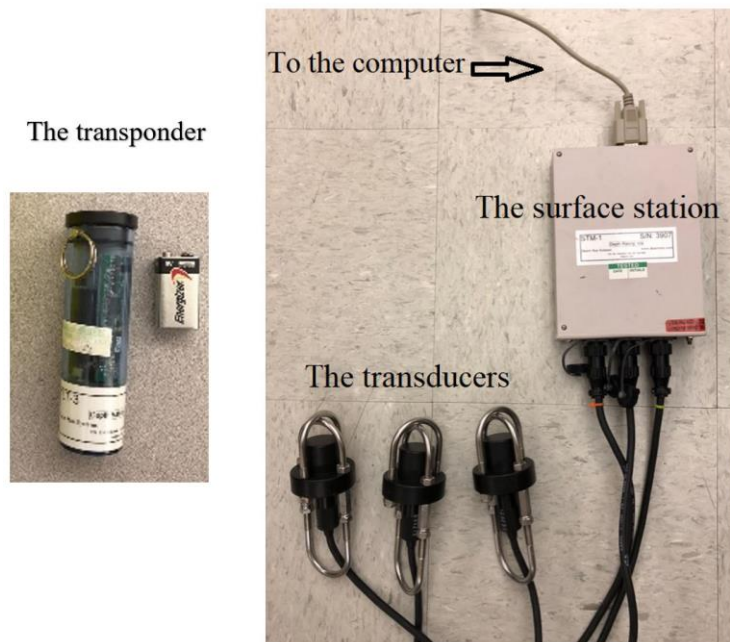


Figure 3.5 The components of the PILOT acoustic positioning system from Desert Star Inc.

The PILOT acoustic positioning system from Desert Star Inc. was used as an external sensor for the experiments. The PILOT system is SBL, and the effective area is within 250m-1000m of the transducers. Moreover, the PILOT system uses high frequency from 34 kHz to 42 kHz. Figure 3.5 is the system components and Figure 3.6 is an image of the system's configuration.

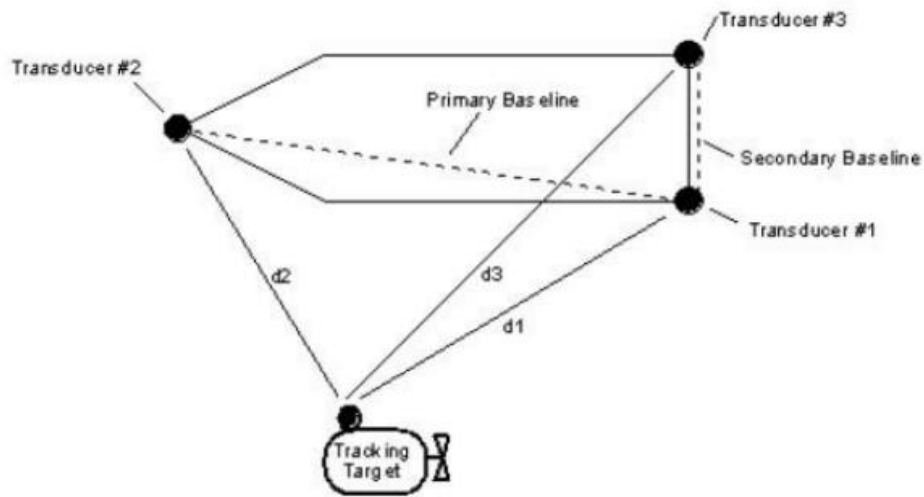


Figure 3.6 SBL configuration. The transponder is attached to tracking a target [41].

The constituents of the PILOT system are that one transponder attaches to the AUV, three transducers (S1, S2, and S3) and a surface station as shown in Figure 3.5. The transponder is called TLT-3, and its maximum depth is 330 meters. The transducers are fixed to three buoys and set at different positions as shown in Figure 3.6.

In the setup, the transponder and the AUV are attached together. The last constituent of the system occurs when the surface station is fixed to the ground and connected remotely to a computer. When the system is live, the position of the AUV can be determined by using the surface station to transmit signals known as interrogation signals through transducer S1. The signal passes through the water until it gets to the

transponder and then the transponder responds to the signal. On the other side of the system, the three transducers are waiting to receive the reply from the transponder. When the reply reaches the surface station transducers, the surface station calculates the time of travel between the initiation of the interrogation from the transducer S1 and the transponder's reply at transducers S1, S2, and S3. The speed of sound in water is a constant, so this can be used to determine the distances (d_1 , d_2 , and d_3) covered by the signals (distance = speed \times time). These distances can then be used to determine the target's position through the use of trigonometry computation [41].

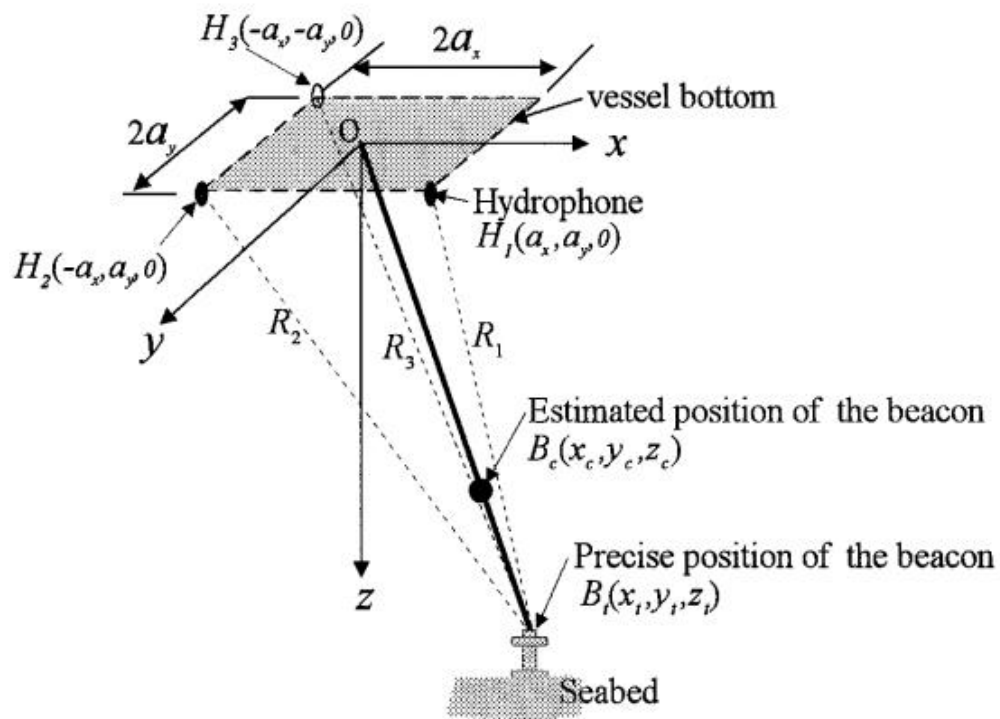


Figure 3.7 Geometry of acoustic propagation with the center of the coordinate in the center of transducers [22].

The locations of each of the three transducers are H_1 , H_2 , and H_3 . They also have their positions in the coordinates as shown in Figure 3.7.

$$H_1 = (a_x, a_y, 0), H_2 = (-a_x, a_y, 0), H_3 = (-a_x, -a_y, 0). \quad (3.27)$$

For this, we will represent the estimated position of the transponder with $B_c = (x_c, y_c, z_c)$, and the distance of the transponder to the three transducers are denoted by R_1 , R_2 , and R_3 . Writing these as a tracking equations, we have:

$$R_1^2 = (x_c - a_x)^2 + (y_c - a_y)^2 + z_c^2 \quad (3.28)$$

$$R_2^2 = (x_c + a_x)^2 + (y_c - a_y)^2 + z_c^2 \quad (3.29)$$

$$R_3^2 = (x_c + a_x)^2 + (y_c + a_y)^2 + z_c^2 \quad (3.30)$$

When we subtract equation 3.29 from equation 3.28 and subtract equation 3.30 with equation 3.29, we yield

$$R_2^2 - R_1^2 = 4x_c a_x \quad (3.31)$$

$$R_3^2 - R_2^2 = 4y_c a_y \quad (3.32)$$

Thus, we can define the estimated position of the transponder as:

$$x_c = \frac{R_2^2 - R_1^2}{4a_x} \quad (3.33)$$

$$y_c = \frac{R_3^2 - R_2^2}{4a_y} \quad (3.34)$$

In the PILOT system, the depth (z) is measured using the pressure sensor which is built-in the transponder [41]. Therefore, when the value of the depth is determined, the transponder transmits it to the transducers.

Important is the fact that the calculation showed above is done by taking into consideration that all the three transducers are in the same plant and proximity close to the water surface.

3.7 Kalman Filter

The Kalman filter (KF) is commonly used for both estimating the states and filtering the measurements. KF uses for linear systems with the Gaussian process and measurement noise [34]. Also, it can be used to reconstruct unmeasured states and remove white and colored noise from the state estimates in sensors and navigation systems [24].

There are several types of Kalman filters, and each type is suitable for a specific system. Hence, they are custom made. The types and their use include:

1. For Linear systems: Discrete-Time Kalman Filter and Continuous-Time Kalman Filter.
2. For non-linear systems: Extended Kalman Filter and Unscented Kalman Filter.

This section is an explanation of the principle behind the Kalman Filter [24].

First, consider the linear continuous-time system (process model):

$$x_k = \mathbf{A}x_{k-1} + \mathbf{B}u_k + \omega_{k-1} \quad (3.36)$$

Where:

k is the time index and $(k - 1)$ is the previous time point.

x_k is the model states vector and might be observable but not measured states.

\mathbf{A} is the process matrix.

\mathbf{B} is the control matrix.

u_k is the input vector.

ω_k is a zero-mean Gaussian white noise vector.

Then, for the measurement model, the number (m) of noisy measurements is denoted by

(z_1, \dots, z_m) and the measurement z_k is represented as:

$$z_k = \mathbf{H}x_k + v_k \quad \text{for } k = 1, \dots, m \quad (3.37)$$

Where \mathbf{H} is Measurement Matrix. Also, the variable x_k is Kalman's Filter will estimate such as positions or velocities. For each k , z_k is the estimated measurement and some references call it y_k . Where the measurement noise is denoted by a random variable v_k and we can state it as $\mathbf{v} = [v_1, v_2, \dots, v_m]$.

The mean and covariance of ω_k and n_k are

$$\begin{aligned} E[\omega_k] &= 0 \quad \text{and} \quad E[v_k] = 0 \\ \mathbf{Q}_k &= E[\omega_k \omega_k^T] \\ \mathbf{R}_k &= E[v_k v_k^T] \end{aligned} \quad (3.38)$$

we define \hat{x}_k^- is the priori state estimate without the measurement available at time k , and \hat{x}_k is the posteriori estimate with the measurement updated at time k . We define two estimated errors: priori estimate errors $e_k^- = x_k - \hat{x}_k^-$ and posterior errors $e_k = x_k - \hat{x}_k$. Thus, the priori estimate error covariance is $P_k^- = E[e_k^- e_k^{-T}]$, and the posteriori estimate error covariance is $P_k = E[e_k e_k^T]$ [42]. The Kalman filter is used to reduce the posteriori estimate error covariance P_k :

$$P_k = E[(x_k - \hat{x}_k)(x_k - \hat{x}_k)^T]. \quad (3.39)$$

And the update equation for the new estimate of the state is stated as:

$$\hat{x}_k = \hat{x}_k^- + K_k(z_k - \mathbf{H}\hat{x}_k^-), \quad (3.40)$$

where K_k is the Kalman gain, and the term $z_k - \mathbf{H}\hat{x}_k^-$ is the innovation or measurement residual.

The equation 3.40 can be updated by substituting z_k with equation 3.37:

$$\hat{x}_k = \hat{x}_k^- + K_k(\mathbf{H}x_k + v_k - \mathbf{H}\hat{x}_k^-). \quad (3.41)$$

Expanding and substituting equation 3.41 into equation 3.39 gives:

$$P_k = E\{[(I - K_k\mathbf{H})(x_k - \hat{x}_k^-) - K_k v_k][(I - K_k\mathbf{H})(x_k - \hat{x}_k^-) - K_k v_k]^T\} \quad (3.42)$$

It is noted that $x_k - \hat{x}_k^-$ is the error of the prior estimate, which means that is uncorrelated with the measurement noise and therefore the expectation can be re-written as [42]:

$$P_k = (I - K_k \mathbf{H}) E[(x_k - \hat{x}_k^-)(x_k - \hat{x}_k^-)^T] (I - K_k \mathbf{H})^T + K_k E[v_k v_k^T] K_k^T \quad (3.43)$$

Plugging Equation 3.39 and 3.38 into 3.43 yields:

$$P_k = (I - K_k \mathbf{H}) P_k^- (I - K_k \mathbf{H})^T + K_k \mathbf{R} K_k^T \quad (3.44)$$

where P_k^- is the prior estimate of P_k . Expansion of equation 3.44 as follows

$$P_k = P_k^- - K_k \mathbf{H} P_k^- - P_k^- \mathbf{H}^T K_k^T + K_k (\mathbf{H} P_k^- \mathbf{H}^T + \mathbf{R}) K_k^T \quad (3.45)$$

Since the goal of the Kalman filter is to find the Kalman gain K which can minimize P_k , the P_k can be minimized by minimizing the trace of P_k . Taking the trace of P_k yields:

$$T[P_k] = T[P_k^-] - 2T[K_k \mathbf{H} P_k^-] + T[K_k (\mathbf{H} P_k^- \mathbf{H}^T + \mathbf{R}) K_k^T], \quad (3.46)$$

where $T[P_k]$ is the trace of the matrix P_k . Differentiating with respect to K_k gives:

$$\frac{dT[P_k]}{dK_k} = -2(\mathbf{H} P_k^-)^T + 2K_k (\mathbf{H} P_k^- \mathbf{H}^T + \mathbf{R}). \quad (3.47)$$

Setting to zero and re-arranging is yielded to

$$(\mathbf{H} P_k^-)^T = K_k (\mathbf{H} P_k^- \mathbf{H}^T + \mathbf{R}) \quad (3.48)$$

Solving for K_k yields

$$K_k = P_k^- \mathbf{H}^T (\mathbf{H} P_k^- \mathbf{H}^T + \mathbf{R})^{-1} \quad (3.49)$$

Equation 3.49 is the Kalman gain expression. Substituting equation 3.49 to 3.45 yield

$$\begin{aligned} P_k &= P_k^- - P_k^- \mathbf{H}^T (\mathbf{H} P_k^- \mathbf{H}^T + \mathbf{R})^{-1} \mathbf{H} P_k^- \\ &= P_k^- - K_k \mathbf{H} P_k^- \\ &= (I - K_k \mathbf{H}) P_k^- \end{aligned} \quad (3.50)$$

Equation 3.50 is the update equation for the error covariance matrix with the Kalman gain. At time index $k - 1$, we can estimate the state \hat{x}_k by using:

$$\hat{x}_k = \mathbf{A} \hat{x}_{k-1} + \mathbf{B} u_k \quad (3.51)$$

and error covariance matrix \hat{P}_k^-

$$\begin{aligned}
 \hat{P}_k^- &= E[(x_k - \hat{x}_k)(x_k - \hat{x}_k)^T] \\
 &= E[[Ax_{k-1} + Bu_k + \omega_{k-1} - (A\hat{x}_{k-1} + Bu_k)][Ax_{k-1} + Bu_k + \omega_{k-1} - (A\hat{x}_{k-1} + Bu_k)]^T] \\
 &= E[A(x_{k-1} - \hat{x}_{k-1})A^T] + E[\omega_{k-1}\omega_{k-1}^T] \\
 &= AP_{k-1}A^T + Q
 \end{aligned} \tag{3.52}$$

Hence, the Kalman filter is a two-step process. The prediction process is done by equations 3.51 and 3.52 and equations 3.40, 3.50 and 3.49 for the update process. Figure 3.8 shows the filter process that has two major stages, which are the prediction and the update.

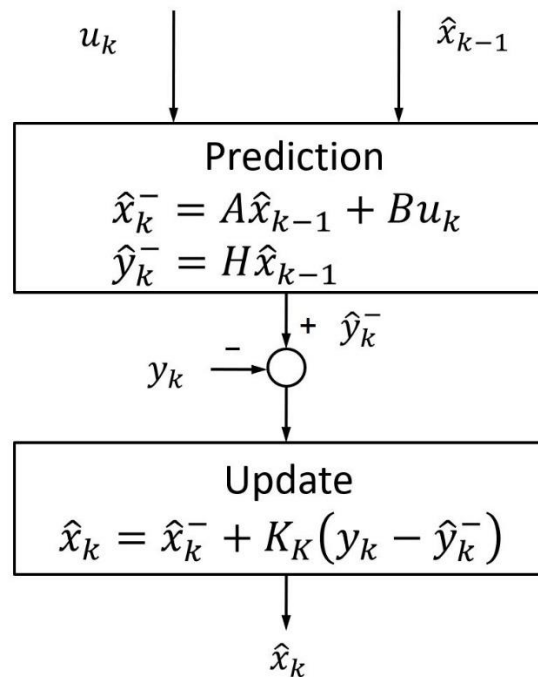


Figure 3.8 Kalman filter process.

3.7.1 The Kalman filter algorithm

To sum up, Table 3.2 below illustrates the algorithm of the Kalman filter.

Table 3.2 The algorithm of the Kalman filter [43].

<ul style="list-style-type: none"> • Step 1 (Initialization): Start with $k = 0$. Initialize the state estimate $\hat{x}_0 = E(x_0)$ (say to zero) and the state covariance estimate $\hat{P}_0 = E(x_0 x_0^T)$ (say to I)
<ul style="list-style-type: none"> • Step 2 (Prediction): Set $k = k + 1$, use u_{k-1}, \hat{x}_{k-1}, \hat{P}_{k-1}, Q_{k-1} to predict the current state \hat{x}_k and its covariance \hat{P}_k^- as $\hat{x}_k^- = \mathbf{A}\hat{x}_{k-1} + \mathbf{B}u_k$ $\hat{P}_k^- = \mathbf{A}P_{k-1}\mathbf{A}^T + \mathbf{Q}$
<ul style="list-style-type: none"> • Step 3 (Filter Update and Estimation): <ul style="list-style-type: none"> – Use \hat{P}_k^- and \mathbf{R} to update the Kalman filter gain K_k by $K_k = P_k^- \mathbf{H}^T (\mathbf{H}P_k^- \mathbf{H}^T + \mathbf{R})^{-1}$ – Use K_k, \hat{x}_k^-, \hat{P}_k^-, and the measurement z_k to estimate the state and its covariance as $\hat{x}_k = \hat{x}_k^- + K_k(z_k - \mathbf{H}\hat{x}_k^-)$ $P_k = (\mathbf{I} - K_k\mathbf{H})P_k^-$
<ul style="list-style-type: none"> • Repeat Steps 2 and 3 until finished.

3.8 Extended Kalman Filter

The Kalman filter discussed above is used only for linear systems. The extended Kalman Filter is what is used for non-linear systems. The concept behind this filter is to make the non-linear system linear and then follow the same KF algorithm. The linearization is done by using the Taylor Series. The notations stay the same as used in KF.

$$f(x) = f(a) + f'(a)(x - a) + H.O.T. \quad (3.53)$$

In the equation above, H.O.T. means the higher order terms. Equation 3.53 shows that by using the Taylor Series expansion, a function can be expanded into a series of sub-functions about a point a . In the EKF, the nonlinear model:

$$\begin{aligned} x_k &= f(x_{k-1}) + \omega_{k-1} \\ z_k &= h(x_k) + v_k \end{aligned} \quad (3.54)$$

Performing a Taylor Series expansion on \hat{x}_{k-1} as follow

$$x_k = f(x_{k-1}) = f(\hat{x}_{k-1}) + J_f(\hat{x}_{k-1})(x_{k-1} - \hat{x}_{k-1}) + H.O.T. \quad (3.55)$$

where J_f is the Jacobian of $f(x_{k-1})$, and the Jacobian define as following

$$J_f = \begin{bmatrix} \frac{\partial f_1}{\partial x_1} & \dots & \frac{\partial f_1}{\partial x_n} \\ \vdots & \ddots & \vdots \\ \frac{\partial f_n}{\partial x_1} & \dots & \frac{\partial f_n}{\partial x_n} \end{bmatrix} \quad (3.56)$$

H.O.T. is negligible in the equation 3.53, and we define

$$e_{k-1} = x_{k-1} - \hat{x}_{k-1} \quad (3.57)$$

Hence, equation 3.55 can be rewritten as:

$$f(x_{k-1}) \approx f(\hat{x}_{k-1}) + J_f(\hat{x}_{k-1})e_{k-1} \quad (3.58)$$

At time $k - 1$, we have z_{k-1} as a measurement. Then, at time k , we can predict the states \hat{x}_k^- by performing the expectation of $f(x_{k-1})$

$$\hat{x}_k^- = E[f(x_{k-1})|z_{k-1}] \approx f(\hat{x}_{k-1}) + J_f(\hat{x}_{k-1})E[e_{k-1}|z_{k-1}] \quad (3.59)$$

where $E[e_{k-1}|z_{k-1}] = 0$ at time $k - 1$. Thus, the priori estimate value of x_k is

$$\hat{x}_k^- \approx f(\hat{x}_{k-1}) \quad (3.60)$$

For the priori estimate error at time k gives:

$$e_k^- = x_k - \hat{x}_k^- \quad (3.61)$$

plugging equations 3.54 and equation 3.60 into equation 3.61 yields:

$$e_k^- = f(x_{k-1}) + \omega_{k-1} - f(\hat{x}_{k-1}) \approx J_f(\hat{x}_{k-1})e_{k-1} + \omega_{k-1} \quad (3.62)$$

The priori estimate error covariance is:

$$\begin{aligned} P_k^- &= E[e_k^- e_k^{-T}] = J_f(\hat{x}_{k-1})E[e_{k-1}e_{k-1}^T]J_f^T(\hat{x}_{k-1}) + E[\omega_{k-1}\omega_{k-1}^T] \\ &= J_f(\hat{x}_{k-1})P_{k-1}J_f^T(\hat{x}_{k-1}) + Q_{k-1} \end{aligned} \quad (3.63)$$

The update equation for the new estimation is given as

$$\hat{x}_k = \hat{x}_k^- + K_k(z_k - E[h(x_k)|z_k]) \quad (3.64)$$

where $E[h(x_k)|z_k]$ is the estimate state with the measurement at time k . We use the Taylor Series expansion to expand $h(x_k)$ about \hat{x}_k^- to yield

$$h(x_k) \approx h(\hat{x}_k^-) + J_h(\hat{x}_k^-)(x_k - \hat{x}_k^-) \quad (3.65)$$

where the Jacobian matrix $J_h(\hat{x}_k^-)$ is defined as

$$J_f = \begin{bmatrix} \frac{\partial h_1}{\partial x_1} & \dots & \frac{\partial h_1}{\partial x_n} \\ \vdots & \ddots & \vdots \\ \frac{\partial h_m}{\partial x_1} & \dots & \frac{\partial h_m}{\partial x_n} \end{bmatrix} \quad (3.66)$$

Given the measurement z_k at time k and taking the expectation on both sides of equation 3.65 give:

$$E[h(x_k)|z_k] \approx h(\hat{x}_k^-) + J_h(\hat{x}_k^-)E[e_k^-|z_k] \quad (3.67)$$

let $E[e_k^-|z_k] = 0$. Then, equation 3.67 can be rewritten as:

$$E[h(x_k)|z_k] \approx h(\hat{x}_k^-) \quad (3.68)$$

Rewrite equation 3.67 with placing equation 3.68

$$\hat{x}_k = \hat{x}_k^- + K_k(z_k - h(\hat{x}_k^-)) \quad (3.69)$$

The error in the estimate \hat{x}_k is:

$$e_k = x_k - \hat{x}_k = f(x_{k-1}) + \omega_{k-1} - \hat{x}_k^- - K_k(z_k - h(\hat{x}_k^-)) \quad (3.70)$$

Plugging equation 3.60 and 3.54 into equation 3.70 yields:

$$e_k \approx f(x_{k-1}) - f(\hat{x}_{k-1}) + \omega_{k-1} - K_k(h(x_k) + v_k - h(\hat{x}_k^-)) \quad (3.71)$$

Rewriting equation 3.71 with adding equations 3.58, 3.61 and 3.65

$$e_k \approx J_f(\hat{x}_{k-1})e_{k-1} + \omega_{k-1} - K_k(J_h(\hat{x}_k^-)e_k + v_k) \quad (3.72)$$

By using equation 3.62, equation 3.72 can be rewritten as

$$\begin{aligned} e_k &\approx J_f(\hat{x}_{k-1})e_{k-1} + \omega_{k-1} - K_k J_h(\hat{x}_k^-)(J_f(\hat{x}_{k-1})e_{k-1} + \omega_{k-1}) - K_k v_k \\ &\approx (I - K_k J_h(\hat{x}_k^-))J_f(\hat{x}_{k-1})e_{k-1} + (I - K_k J_h(\hat{x}_k^-))\omega_{k-1} - K_k v_k \end{aligned} \quad (3.73)$$

Since we have the posteriori estimate error, we can get the posteriori estimate error covariance as following

$$\begin{aligned}
P_k &= E[e_k e_k^T] \\
&= (I - K_k J_h(\hat{x}_k^-)) J_f(\hat{x}_{k-1}) P_{k-1} J_f^T(\hat{x}_{k-1}) (I - K_k J_h(\hat{x}_k^-))^T + \\
&\quad (I - K_k J_h(\hat{x}_k^-)) Q_{k-1} (I - K_k J_h(\hat{x}_k^-))^T + K_k R_k K_k^T \quad (3.74)
\end{aligned}$$

Plugging equation 3.63 into equation 3.74 yields

$$\begin{aligned}
P_k &= (I - K_k J_h(\hat{x}_k^-)) P_k^- (I - K_k J_h(\hat{x}_k^-))^T + K_k R_k K_k^T \\
&= P_k^- - K_k J_h(\hat{x}_k^-) P_k^- - P_k^- J_h(\hat{x}_k^-) K_k^T + K_k J_h(\hat{x}_k^-) P_k^- J_h^T(\hat{x}_k^-) K_k^T + K_k R_k K_k^T \quad (3.75)
\end{aligned}$$

The goal of EKF is picking the Kalman gain that can minimize the posteriori estimate error covariance. Therefore, to find the Kalman gain K_k , we take the derivate of the trace of P_k and equal it with zero to find the Kalman gain K_k

$$0 = \frac{\partial T[P_k]}{\partial K_k} = -(J_h(\hat{x}_k^-) P_k^-)^T - P_k^- J_h^T(\hat{x}_k^-) + 2K_k J_h(\hat{x}_k^-) P_k^- J_h^T(\hat{x}_k^-) + 2K_k R_k \quad (3.76)$$

Then the Kalman gain is

$$K_k = P_k^- J_h^T(\hat{x}_k^-) (J_h(\hat{x}_k^-) P_k^- J_h^T(\hat{x}_k^-) + R_k)^{-1} \quad (3.77)$$

Now, we can plug equation 3.77 back into equation 3.75

$$P_k = (I - K_k J_h(\hat{x}_k^-)) P_k^- \quad (3.78)$$

Hence, there are two processes of the EKF as shown in Table 3.3.

Table 3.3 The EKF process.

Prediction	$\hat{x}_k^- = f(\hat{x}_{k-1}, u_{k-1})$ $\hat{P}_k^- = J_f(\hat{x}_{k-1}) \hat{P}_{k-1} J_f^T(\hat{x}_{k-1}) + Q$
Filter update	$K_k = \hat{P}_k^- J_h^T(\hat{x}_k^-) (J_h(\hat{x}_k^-) \hat{P}_k^- J_h^T(\hat{x}_k^-) + R)^{-1}$ $\hat{x}_k = \hat{x}_k^- + K_k (z_k - h(\hat{x}_k^-))$ $\hat{P}_k = (I - K_k J_h(\hat{x}_k^-)) \hat{P}_k^-$

3.8.1 Extended Kalman Filter algorithm

The Table 3.4 below illustrates the algorithm of the Extended Kalman filter.

Table 3.4 The algorithm of the Extended Kalman Filter [43].

<ul style="list-style-type: none"> • Step 1 (Initialization): Start with $k = 0$. Initialize the state estimate $\hat{x}_0 = E(x_0)$ (say to zero) and the state covariance estimate $\hat{P}_0 = E(x_0 x_0^T)$ (say to I)
<ul style="list-style-type: none"> • Step 2 (Linearize State Prediction Matrix): Set $k = k + 1$, use \hat{x}_{k-1}, u_{k-1} to find A_k.
<ul style="list-style-type: none"> • Step 3 (Prediction): Use $u_{k-1}, \hat{x}_{k-1}, \hat{P}_{k-1}, Q_{k-1}, A_k$ to predict the current state \hat{x}_k^- and its covariance \hat{P}_k^- as $\hat{x}_k^- = f(\hat{x}_{k-1}, u_{k-1})$ $\hat{P}_k^- = A_k \hat{P}_{k-1} A^T + Q_{k-1}$
<ul style="list-style-type: none"> • Step 4 (Linearize Measurement Prediction Matrix): use \hat{x}_k^- to determine H_k.
<ul style="list-style-type: none"> • Step 5 (Filter Update and Estimation) <ul style="list-style-type: none"> – Use \hat{P}_k^- and R_k to update the Kalman filter gain K_k by $K_k = \hat{P}_k^- H_k^T (H_k \hat{P}_k^- H_k^T + R_k)^{-1}$ – Use $K_k, \hat{x}_k^-, \hat{P}_k^-$, and the measurement y_k to estimate the state and its covariance as $\hat{x}_k = \hat{x}_k^- + K_k (y_k - h(\hat{x}_k^-))$ $\hat{P}_k = (I - K_k H_k) \hat{P}_k^-$
<ul style="list-style-type: none"> • Repeat Steps 2 through 5 until finished

EKF has some disadvantages such as the difficulty of tuning, and when dealing with highly non-linear systems, its estimations will be unreliable for the states. This is due to the covariance distributed as a result of the linearization of the non-linear model. Due to this inability, the Unscented Kalman Filter was developed [42].

3.9 Unscented Kalman Filter

When the EKF is linearizing non-linear models, there are events of information loss because of selecting only the first order term of the Taylor Series. This can cause an error in the estimated states. Therefore, the Unscented Kalman Filter can avoid this. The

state distribution is denoted by a small set of randomly and carefully selected sample points. These points are referred to as sigma points. The mean value of the sigma points is equivalent to the mean value of the states. The same applies to the covariance values. Hence, the UKF propagates sigma positions through the original nonlinear model rather than how the EKF propagates whole states in the linearized model.

Consequently, the basic idea of the UKF is the estimation of the states of a system by using unscented transformation. The unscented transformation helps to determine the statistics of a random variable that has gone through a nonlinear transformation. To show the unscented transformation, let us denote the sigma point with \mathfrak{X} [44].

$$\mathfrak{X} = [x, x + \sqrt{P_x}\sqrt{L + \lambda}, x - \sqrt{P_x}\sqrt{L + \lambda}] \quad (3.79)$$

Where

x is the vector of states.

L is the number of states.

λ is a scaling parameter, and it is calculated by

$$\lambda = \alpha^2 * (L + k) - L \quad (3.80)$$

where α is the spread of sigma points around states x , and its range is from 10^{-4} to 1.

The small value of α means sigma points are close to states x , and large α gives wide spread. k is secondary scaling parameter which is usually set to 0.

Now, we can mathematically define the unscented transformation φ after we presented the definition of the sigma points.

$$\varphi = f(\mathfrak{X}) \quad (3.81)$$

where $f(\mathfrak{X})$ is a nonlinear model.

The mean of the unscented transformation is defined by

$$y = \sum_{i=0}^{2L} n_i^m * \varphi_i \quad (3.82)$$

where

$$n_i^m = \begin{cases} \frac{\lambda}{L+\lambda}; & i = 0 \\ \frac{1}{2(L+\lambda)}; & i = 1, 2, \dots, 2L. \end{cases} \quad (3.83)$$

Also, the covariance of the unscented transformation is

$$P_y = \sum_{i=0}^{2L} n_i^c * (\varphi_i - y) * (\varphi_i - y)^T \quad (3.84)$$

where

$$n_i^c = \begin{cases} \frac{\lambda}{L+\lambda} + 1 - \alpha^2 + \beta; & i = 0 \\ \frac{1}{2(L+\lambda)}; & i = 1, 2, \dots, 2L. \end{cases} \quad (3.85)$$

Where β provides information about the prior knowledge of the distribution of x . If the distribution is Gaussian distribution, then β equals to 2.

In the UKF's algorithm, first, we need to define nonlinear models for process model and measurement model as following

$$\hat{x}_k^- = f(\hat{x}_{k-1}, u_{k-1}) + w_{k-1} \quad (3.86)$$

$$y_k = h(\hat{x}_{k-1}, u_{k-1}) + v_{k-1} \quad (3.87)$$

Then, we need to define the sigma points

$$\mathfrak{X}_{k-1} = [\hat{x}_{k-1}, \hat{x}_{k-1} + \sqrt{L + \lambda} \sqrt{P_{k-1}}, \hat{x}_{k-1} - \sqrt{L + \lambda} \sqrt{P_{k-1}}] \quad (3.88)$$

Next, we need to propagate sigma points in nonlinear models, which are the prediction model and the measurement model.

First, we propagate the sigma points in the prediction model

$$\mathfrak{X}_k^i = f(\mathfrak{X}_{k-1}, u_{k-1}), \quad i = 0, 1, 2, \dots, 2L \quad (3.89)$$

The mean of the predicted state is presented as

$$y = \hat{x}_k^- = \sum_{i=0}^{2L} n_i^m * \mathfrak{N}_k^i, \quad (3.90)$$

and the covariance of the predicted state is defined as

$$P_y = P_k^- = \sum_{i=0}^{2L} n_i^c * (\mathfrak{N}_k^i - \hat{x}_k^-)(\mathfrak{N}_k^i - \hat{x}_k^-)^T + Q_{k-1} \quad (3.91)$$

Secondly, we propagate sigma points in the observation model

$$Y_k^- = h(\mathfrak{N}_k, u_k) \quad (3.92)$$

The mean of the predicted output is

$$\hat{y}_k^- = \sum_{i=0}^{2L} n_i^m Y_k^- \quad (3.93)$$

and the covariance of predicted output is defined as

$$P_k^{yy} = R_k + \sum_{i=0}^{2k} n_i^c (Y_k^- - \hat{y}_k^-)(Y_k^- - \hat{y}_k^-)^T \quad (3.94)$$

and the cross-covariance between state and output is defined as

$$P_k^{xy} = \sum_{i=0}^{2L} n_i^c (\mathfrak{N}_k^i - \hat{x}_k^-)(Y_k^- - \hat{y}_k^-)^T \quad (3.95)$$

The update processes of the UKF are

1. Calculate Kalman gain K

$$K = P_k^{xy} (P_k^{yy})^{-1} \quad (3.96)$$

2. Update states estimate

$$\hat{x}_k = \hat{x}_k^- + K * (y_k - \hat{y}_k^-) \quad (3.97)$$

3. Update covariance estimate

$$P_k = P_k^- - K P_k^{yy} K^T \quad (3.98)$$

UKF has two major steps as the KF and EKF, which are the prediction and the update, and these two steps are shown in the table below.

Table 3.5 The Unscented Kalman Filter's algorithm.

Prediction	$\hat{x}_k^- = f(\hat{x}_{k-1}, u_{k-1}) + w_{k-1}$ $P_k^- = \sum_{i=0}^{2L} n_i^c * (\mathfrak{N}_k^i - \hat{x}_k^-)(\mathfrak{N}_k^i - \hat{x}_k^-)^T + Q_{k-1}$
Update	$\hat{x}_k = \hat{x}_k^- + K * (y_k - \hat{y}_k^-)$ $K = P_k^{xy} (P_k^{yy})^{-1}$ $P_k = P_k^- - K P_k^{yy} K^T$

3.10 Summary of Three Kalman Filters

This is a comparative analysis of the three filters. A standard feature of all three filters is that they first predict and then update. In the prediction phase, the state and covariance can be calculated using the process model. After the measurement is gotten, the prediction of the state and covariance is now updated. The table below compares these three filters stages and equations.

Table 3.6 The comparison of the three filters.

	Prediction	Update
KF	$\hat{x}_k = \mathbf{A}\hat{x}_{k-1} + \mathbf{B}u_k$ $P_k^- = \mathbf{A}P_{k-1}\mathbf{A}^T + Q_k$	$K_k = P_k^- \mathbf{H}^T (\mathbf{H}P_k^- \mathbf{H}^T + R_k)^{-1}$ $\hat{x}_k = \hat{x}_k^- + K_k(z_k - \mathbf{H}\hat{x}_k^-)$ $P_k = (I - K_k \mathbf{H})P_k^-$
EKF	$\hat{x}_k^- = f(\hat{x}_{k-1}, u_{k-1})$ $P_k^- = J_f(\hat{x}_{k-1})P_{k-1}J_f^T(\hat{x}_{k-1}) + Q_{k-1}$	$\hat{x}_k = \hat{x}_k^- + K_k(z_k - h(\hat{x}_k^-))$ $K_k = P_k^- J_h^T(\hat{x}_k^-) (J_h(\hat{x}_k^-)P_k^- J_h^T(\hat{x}_k^-) + R_k)^{-1}$ $P_k = (I - K_k J_h(\hat{x}_k^-))P_k^-$
UKF	$\hat{x}_k^- = f(\hat{x}_{k-1}, u_{k-1}) + w_{k-1}$ $P_k^- = \sum_{i=0}^{2L} n_i^c * (\mathfrak{N}_k^i - \hat{x}_k^-)(\mathfrak{N}_k^i - \hat{x}_k^-)^T + Q_{k-1}$	$\hat{x}_k = \hat{x}_k^- + K * (y_k - \hat{y}_k^-)$ $K = P_k^{xy} (P_k^{yy})^{-1}$ $P_k = P_k^- - K P_k^{yy} K^T$

EKF and UKF are for nonlinear systems. While the EKF first linearizes the system by calculating the Jacobian forms of nonlinear models and propagating the predictions and covariance of states in linearized models, the UKF propagates sigma points in the nonlinear model without linearizing the system.

3.10.1 The error variance Q and R

All three types of filters have Q and R . Q is identified as the process noise, and it can be found by feeding the system a series of inputs and the model the same inputs. Then, using the differences, the covariance can be estimated. R is known as the measurement noise, and it can be calculated by comparing the outputs of the sensors to the true measurements [43]. To sum up, Q and R must be chosen based on how accurate the model and measurements are.

The error variance Q and R in all three algorithms are used to tune the state-estimate gain for new measurements that will be taken in future. This adjustment is called the Kalman gain K . It is an important part of the Kalman Filter algorithm. It affects the weight between priori prediction \hat{x}_k^- and residual $z_k - h(\hat{x}_k^-)$.

Looking at the equation for calculating Kalman gain in each algorithm, when the measurement error covariance R be close to zero, the gain K weights the residual more heavily [42]. To illustrate, we use KF as an example. When R approaches zero, the Kalman gain will be

$$\lim_{R_k \rightarrow 0} K_k = \mathbf{H}^{-1} \quad (3.99)$$

Using this Kalman gain value in the update equation, we find

$$\hat{x}_k = \frac{z_k}{\mathbf{H}} \quad (3.100)$$

From the above, the current time estimation relies only on the measurements z_k . On the contrary, as the priori estimate error covariance P_k^- approaches zero, the gain K weights the residual less heavily.

$$\lim_{P_k^- \rightarrow 0} K_k = 0 \quad (3.101)$$

Using this Kalman gain value in the new equation, we got

$$\hat{x}_k = \hat{x}_k^- \quad (3.102)$$

Therefore, in this case, the Kalman Filter relies on the prediction \hat{x}_k^- because the prediction is close to the true states.

3.11 EKF Application for the AUV Navigation

Here, we look at how the EKF is used for AUV navigation. For this application, we would select the states that need to estimate. This project (Yellowfinn II) used nine states

$$\bar{x} = \begin{bmatrix} X \\ Y \\ Z \\ u \\ v \\ w \\ \phi \\ \theta \\ \psi \end{bmatrix} \quad (3.103)$$

At time k , the nine states can be predicted and their previous estimation $k - 1$, and this prediction follows the process model

$$\begin{bmatrix} X \\ Y \\ Z \\ u \\ v \\ w \\ \phi \\ \theta \\ \psi \end{bmatrix}_k = \begin{bmatrix} X_{k-1} + (u_{k-1}c\theta c\psi + v_{k-1}(s\phi s\theta c\psi - c\phi s\psi) + w_{k-1}(c\phi s\theta c\psi + s\phi s\psi))dt \\ Y_{k-1} + (u_{k-1}c\theta s\psi + v_{k-1}(s\phi s\theta s\psi + c\phi c\psi) + w_{k-1}(c\phi s\theta s\psi - s\phi c\psi))dt \\ Z_{k-1} + (-u_{k-1}s\theta + v_{k-1}s\phi c\theta + w_{k-1}c\phi c\theta)dt \\ u_{k-1} + a_{x_{k-1}}dt \\ v_{k-1} + a_{y_{k-1}}dt \\ w_{k-1} + a_{z_{k-1}}dt \\ \phi_{k-1} + (p_{k-1} + q_{k-1}s\phi t\theta + r_{k-1}c\phi t\theta)dt \\ \theta_{k-1} + (q_{k-1}c\phi - r_{k-1}s\phi)dt \\ \psi_{k-1} + (q_{k-1}s\phi sec\theta + r_{k-1}c\phi sec\theta)dt \end{bmatrix} \quad (3.104)$$

where $s = \sin$, $c = \cos$ and $t = \tan$.

In the above equation, $a_x, a_y, a_z, p, q,$ and r are inputs for the EKF, and their values are the measurements of the IMU. The Jacobian matrix of the above model is shown in the matrix below (Equation 3.105)

$$J = \begin{bmatrix} 1 & 0 & 0 & c\theta c\psi dt & (s\phi s\theta c\psi - c\phi s\psi)dt & (c\phi s\theta c\psi + s\phi s\psi)dt & J_f(1,10) & J_f(1,11) & J_f(1,12) \\ 0 & 1 & 0 & c\theta s\psi dt & (s\phi s\theta s\psi + c\phi c\psi)dt & (c\phi s\theta s\psi - s\phi c\psi)dt & J_f(2,10) & J_f(2,11) & J_f(2,12) \\ 0 & 0 & 1 & -s\theta dt & s\phi c\theta dt & c\phi c\theta dt & J_f(3,10) & J_f(3,11) & J_f(3,12) \\ 0 & 0 & 0 & 1 & 0 & 0 & 0 & 0 & 0 \\ 0 & 0 & 0 & 0 & 1 & 0 & 0 & 0 & 0 \\ 0 & 0 & 0 & 0 & 0 & 1 & 0 & 0 & 0 \\ 0 & 0 & 0 & 0 & 0 & 0 & J_f(10,10) & J_f(10,11) & J_f(10,12) \\ 0 & 0 & 0 & 0 & 0 & 0 & J_f(11,10) & J_f(11,11) & J_f(11,12) \\ 0 & 0 & 0 & 0 & 0 & 0 & J_f(12,10) & J_f(12,11) & J_f(12,12) \end{bmatrix}$$

where

$$\begin{bmatrix} J_f(1,10) \\ J_f(1,11) \\ J_f(1,12) \end{bmatrix} = \begin{bmatrix} 0 & c\phi s\theta c\psi + s\phi s\psi & -s\phi s\theta c\psi + c\phi s\psi \\ -s\theta c\psi & s\phi c\theta c\psi - c\phi s\psi & c\phi c\theta c\psi + s\phi s\psi \\ 0 & c\phi s\theta c\psi + s\phi s\psi & -s\phi s\theta c\psi + c\phi s\psi \end{bmatrix} \begin{bmatrix} u_{k-1} \\ v_{k-1} \\ w_{k-1} \end{bmatrix} dt$$

$$\begin{bmatrix} J_f(2,10) \\ J_f(2,11) \\ J_f(2,12) \end{bmatrix} = \begin{bmatrix} 0 & c\phi s\theta s\psi - s\phi c\psi & s\phi s\theta s\psi - c\phi c\psi \\ -s\theta s\psi & s\phi c\theta s\psi + c\phi c\psi & c\phi c\theta s\psi - s\phi c\psi \\ c\theta c\psi & s\phi s\theta c\psi - c\phi s\psi & c\phi s\theta c\psi + s\phi s\psi \end{bmatrix} \begin{bmatrix} u_{k-1} \\ v_{k-1} \\ w_{k-1} \end{bmatrix} dt$$

$$\begin{bmatrix} J_f(3,10) \\ J_f(3,11) \\ J_f(3,12) \end{bmatrix} = \begin{bmatrix} 0 & c\phi c\theta & -s\phi c\theta \\ -c\theta & -s\phi s\theta & -c\phi s\theta \\ 0 & 0 & 0 \end{bmatrix} \begin{bmatrix} u_{k-1} \\ v_{k-1} \\ w_{k-1} \end{bmatrix} dt$$

$$\begin{bmatrix} J_f(10,10) \\ J_f(10,11) \\ J_f(10,12) \end{bmatrix} = \begin{bmatrix} 1 \\ 0 \\ 0 \end{bmatrix} + \begin{bmatrix} 0 & c\phi t\theta & -s\phi t\theta \\ 0 & s\phi(t^2\theta + 1) & -c\phi c\theta \\ 0 & 0 & 0 \end{bmatrix} \begin{bmatrix} p_{k-1} \\ q_{k-1} \\ r_{k-1} \end{bmatrix} dt$$

$$\begin{bmatrix} J_f(11,10) \\ J_f(11,11) \\ J_f(11,12) \end{bmatrix} = \begin{bmatrix} 0 \\ 1 \\ 0 \end{bmatrix} + \begin{bmatrix} 0 & -s\phi & c\phi \\ 0 & 0 & 0 \\ 0 & 0 & 0 \end{bmatrix} \begin{bmatrix} p_{k-1} \\ q_{k-1} \\ r_{k-1} \end{bmatrix} dt$$

$$\begin{bmatrix} J_f(12,10) \\ J_f(12,11) \\ J_f(12,12) \end{bmatrix} = \begin{bmatrix} 0 \\ 0 \\ 1 \end{bmatrix} + \begin{bmatrix} 0 & c\phi \sec\theta & -s\phi \sec\theta \\ 0 & s\phi \sec\theta t\theta & c\phi \sec\theta t\theta \\ 0 & 0 & 0 \end{bmatrix} \begin{bmatrix} p_{k-1} \\ q_{k-1} \\ r_{k-1} \end{bmatrix} dt$$

When the system does not have SBL system's information updating, the measurement vector \bar{y}_k will be

$$\bar{y}_k = [Z, u, v, w, \phi, \theta, \psi]^T \quad (3.106)$$

and the observation model becomes

$$\begin{bmatrix} Z \\ u \\ v \\ w \\ \phi \\ \theta \\ \psi \end{bmatrix}_k = \begin{bmatrix} 0 & 0 & 1 & 0 & 0 & 0 & 0 & 0 & 0 \\ 0 & 0 & 0 & 1 & 0 & 0 & 0 & 0 & 0 \\ 0 & 0 & 0 & 0 & 1 & 0 & 0 & 0 & 0 \\ 0 & 0 & 0 & 0 & 0 & 1 & 0 & 0 & 0 \\ 0 & 0 & 0 & 0 & 0 & 0 & 1 & 0 & 0 \\ 0 & 0 & 0 & 0 & 0 & 0 & 0 & 1 & 0 \\ 0 & 0 & 0 & 0 & 0 & 0 & 0 & 0 & 1 \end{bmatrix} \begin{bmatrix} X \\ Y \\ Z \\ u \\ v \\ w \\ \phi \\ \theta \\ \psi \end{bmatrix}_k \quad (3.107)$$

In the measurement vector, the depth Z is measured from the pressure sensor that built-in the DVL, linear velocities u, v, w are measured from the DVL, and ϕ, θ, ψ are measured from the IMU's embedded EKF.

3.12 UKF Application for the AUV Navigation

Here, we discussed how the UKF algorithm is applied in the AUV navigation.

Similar to the first step in the EKF, we define the state vector as

$$\bar{x} = [X, Y, Z, u, v, w, \phi, \theta, \psi]^T \quad (3.108)$$

In exchange for the propagating states for the process model, we would propagate sigma points in the process model. Recall the sigma point (equation 3.88)

$$\mathbf{x}_{k-1} = [\hat{x}_{k-1}, \hat{x}_{k-1} + \sqrt{L + \lambda} \sqrt{P_{k-1}}, \hat{x}_{k-1} - \sqrt{L + \lambda} \sqrt{P_{k-1}}]$$

where \hat{x}_{k-1} is the previous estimated states vector. Since we have nine states in the state vector, the number of states L equals to 9. Primary scaling parameter α equals to 1, and k equals to 0. Recall equation (3.80) for calculating λ

$$\lambda = \alpha^2 * (L + k) - L$$

In this experiment, λ equals to 0 for Yellowfinn II. After we have the value of λ and α ,

we can calculate the weighting factors n_i^m and n_i^c (Equations 3.83 and 3.85)

$$n_i^m = \begin{cases} \frac{\lambda}{L+\lambda} = 0; & i = 0 \\ \frac{1}{2(L+\lambda)} = \frac{1}{18}; & i = 1, 2, \dots, 18, \end{cases}$$

$$n_i^c = \begin{cases} \frac{\lambda}{L+\lambda} + 1 - \alpha^2 + \beta = 2; & i = 0 \\ \frac{1}{2(L+\lambda)} = \frac{1}{18}; & i = 1, 2, \dots, 18. \end{cases}$$

Now, we can update the expression of sigma points with values of the L and λ

$$\mathfrak{X}_{k-1} = [\hat{x}_{k-1}, \hat{x}_{k-1} + 3\sqrt{P_{k-1}}, \hat{x}_{k-1} - 3\sqrt{P_{k-1}}]$$

UKF and EKF algorithms have the same process model and observation models.

However, in the UKF's algorithm, the sigma points are propagated instead of states in the process and observation models.

Chapter IV

Results

This thesis is aimed to study and test the combined navigation method. The proposed method is a combination of IMU and the acoustic positioning system (SBL). The errors often grow in an abnormal manner in the integration process. Thus, this is one of the limitations of INS. However, the SBL acoustic can replace the traditional GPS signals to provide an external position of the AUV. The measurements of sensors are fused together by using EKF or UKF. Therefore, accurate information about the position is calculated based on the estimated states.

This chapter presents the simulations and the results of the experiments of the combined navigation method.

4.1 The Measurements Error Covariance

The stationary test was carried out before the implementation of simulations and experiments. This stationary test provided the measurements error covariance. To do this test, Yellowfinn II was dipped into a water tank, which was completely full of water. Then, the calculations and measurements were recorded when the Yellowfinn II was entirely in water. The measurements were collected from the inertial sensors, which are the IMU and DVL. Yellowfinn II was stagnant in the water tank, and there was no movement. Theoretically, the measurements had to be zero from the inertial sensors since the AUV did not move at all. However, there were uncertainties and imperfections, so the inertial sensors measurements were not zero, but they were very close to zero. Therefore, these differences were considered as the errors of inertial sensors and used in the measurements noise covariance matrix \mathbf{R} in the KF, EKF, and UKF. Figure 4.1 shows the

Yellowfin II in a tank of water for the stationary test to collect the errors in the inertial sensors' measurements.



Figure 4.1 The stationary test for Yellowfin II [22].

There were around 105,000 recordings had been collected from the inertial sensors for the stationary test. Figure 4.2 illustrates these measurements, which are the velocities, accelerations, and angular rates of the Yellowfin II. Additionally, all these measurements are in the Body-fixed frame except the measurements for the pressure sensor are in the NED frame. The pressure sensor is used to measure the depth.

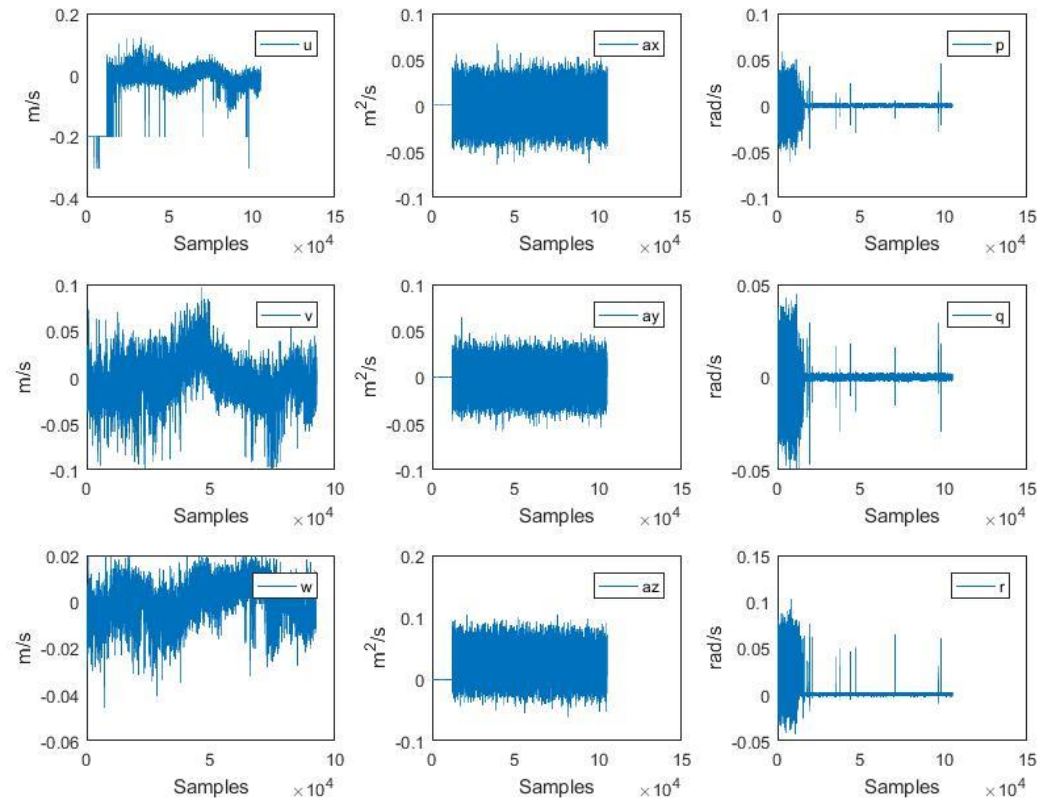


Figure 4.2 The measurements of the stationary test from the inertial sensors.

The diagram clearly depicts that the inertial sensors were very close to zero. The velocity was measured from the DVL, and all values taken had been within the range of 0.2 m/s . The acceleration and angular rates were calculated from the IMU and were within the range of $0.1 \text{ m}^2/\text{s}$ and 0.05 rad/s respectively. The different variances of all the calculations are described below in Table 4.1.

Table 4.1 The variance of measurements from the inertial sensors.

Measurements	Variance
Velocity in the x direction	4.462050928810e-04
Velocity in the y direction	4.581253408175e-04
Velocity in the z direction	5.589327163808e-05
Acceleration in the x direction	1.734044457218e-04
Acceleration in the y direction	1.386420127628e-04
Acceleration in the z direction	3.902668020873e-04
Angular rate in x direction	2.380938812720e-05
Angular rate in y direction	1.942083507151e-05
Angular rate in z direction	1.110844405135e-04
Roll from the IMU's embedded EKF	6.479969606769e-04
Pitch from the IMU's embedded EKF	9.357860293785e-05
Yaw from the IMU's embedded EKF	1.891587893353e-01
Depth from pressure sensor	2.163138935840e-03

The measurements of the attitude angles, which are roll, pitch, and yaw, are derived from the EKF which is embedded with IMU. By using these different variances from Table 4.1, the measurements error covariance matrix \mathbf{R} can be determined as following

$$\mathbf{R} = \begin{bmatrix} 2.16e-3 & 0 & 0 & 0 & 0 & 0 & 0 \\ 0 & 4.46e-4 & 0 & 0 & 0 & 0 & 0 \\ 0 & 0 & 4.58e-4 & 0 & 0 & 0 & 0 \\ 0 & 0 & 0 & 5.58e-5 & 0 & 0 & 0 \\ 0 & 0 & 0 & 0 & 6.48e-4 & 0 & 0 \\ 0 & 0 & 0 & 0 & 0 & 9.36e-5 & 0 \\ 0 & 0 & 0 & 0 & 0 & 0 & 1.89e-1 \end{bmatrix} \quad (4.1)$$

All the sensors measurements are not related to each other. Thus, illustrated that other sensors would not influence the other sensors measurements. The matrix \mathbf{R} can be used for different types of algorithms of KF such as EKF and UKF that were used on the experiments and simulations. However, this matrix can only be used for the INS navigation system, but it cannot be used for the INS/SBL navigation approach of fusion. For the INS/SBL navigation approach, two more diagonal parameters were added. The different parameters added were in the X and Y directions and were known as parameters of variance, and their values can be derived from the SBL.

4.2 The INS and SBL Simulation

The simulation was conducted to verify the performance of navigation system of AUV, the Kalman filter and to compare the simulation output with experimental data. The simulation consists of the true trajectory generator, the measurements generator, and the estimated trajectory generator. The measurements are coming from three sensors: the inertial sensors IMU and DVL, and the external sensor SBL the acoustic positioning system. Generating the true trajectory is done in a simple way such as sine wave, a circle or a straight line, which trajectories were created and considered as the true trajectory of AUV.

Each sensor has its frequency and measurements error covariance. IMU measurements were conducted with 10 Hz. DVL using low update rate around 2Hz. SBL has a low and unstable update rate. In this case, we generated an update rate randomly between [0.5 - 1] Hz for SBL and to match it with other sensor measurements, some of the measurements have been duplicated randomly. That indicates no new measurements for the duplicated measurements. A white Gaussian noise has been added to the measurement trajectories to simulate the real measurements.

The simulation shows the true trajectory, the measurement trajectory, and the KF trajectory. For the true trajectory, we will use different paths such as sine wave, a circle, and a straight line, where the sensors measurements are defined as follows

$$\textit{the measurement} = \textit{the true value} + \textit{Noise}$$

Where the noise is a white noise that has a zero mean, and each sensor has different noise values that usually depend on its variance and other factors.

To perform the simulation, first, we need to define the system model and Kalman filter parameters. Note that all states values are in the NED (Global) frame. Also, the system states are

$$x = \begin{bmatrix} X \\ Y \\ V_x \\ V_y \end{bmatrix} \quad (4.2)$$

For the algorithm of the Kalman filter, Table 3.2 has been used to estimate the states.

Recall equations 3.51 and 3.52 that are used for the prediction process and 3.40, 3.50 and 3.49 that are used for the update process.

For the prediction process, we use u_{k-1} , \hat{x}_{k-1} , \hat{P}_{k-1} , Q_{k-1} to predict the current state \hat{x}_k and its covariance \hat{P}_k^- as

$$\hat{x}_k^- = \mathbf{A}\hat{x}_{k-1} + \mathbf{B}u_k \quad (4.3)$$

$$\hat{P}_k^- = \mathbf{A}\hat{P}_{k-1}\mathbf{A}^T + \mathbf{Q} \quad (4.4)$$

Where

$$u_k = \begin{bmatrix} a_x \\ a_y \end{bmatrix}, \text{ which is the input vector} \quad (4.5)$$

$$\mathbf{A} = \begin{bmatrix} 1 & 0 & T & 0 \\ 0 & 1 & 0 & T \\ 0 & 0 & 1 & 0 \\ 0 & 0 & 0 & 1 \end{bmatrix}, \text{ which is the process matrix, and T is a sample time.} \quad (4.6)$$

$$\mathbf{B} = \begin{bmatrix} 0 & 0 \\ 0 & 0 \\ T & 0 \\ 0 & T \end{bmatrix} \quad (4.7)$$

The process noise matrix is

$$\mathbf{Q} = \begin{bmatrix} \sigma_X^2 & 0 & 0 & 0 \\ 0 & \sigma_Y^2 & 0 & 0 \\ 0 & 0 & \sigma_{V_x}^2 & 0 \\ 0 & 0 & 0 & \sigma_{V_y}^2 \end{bmatrix}, \text{ where } \sigma^2 \text{ is the process variance.} \quad (4.8)$$

Then, for the filter update process, we use \hat{P}_k^- and \mathbf{R} to update the Kalman filter gain K_k by using the following equation

$$K_k = P_k^- \mathbf{H}^T (\mathbf{H} P_k^- \mathbf{H}^T + \mathbf{R})^{-1} \quad (4.9)$$

Where \mathbf{H} is measurement matrix

$$\mathbf{H} = \begin{bmatrix} 1 & 0 & 0 & 0 \\ 0 & 1 & 0 & 0 \\ 0 & 0 & 1 & 0 \\ 0 & 0 & 0 & 1 \end{bmatrix} \quad (4.10)$$

And \mathbf{R} is the measurements noise matrix

$$\mathbf{R} = \begin{bmatrix} \sigma_X^2 & 0 & 0 & 0 \\ 0 & \sigma_Y^2 & 0 & 0 \\ 0 & 0 & \sigma_{V_x}^2 & 0 \\ 0 & 0 & 0 & \sigma_{V_y}^2 \end{bmatrix}, \text{ where } \sigma^2 \text{ is the measurements variance.} \quad (4.11)$$

Next, we use K_k , \hat{x}_k^- , \hat{P}_k^- , and the measurement y_k to estimate the state and its covariance as

$$\hat{x}_k = \hat{x}_k^- + K_k (y_k - \mathbf{H} \hat{x}_k^-) \quad (4.12)$$

$$P_k = (I - K_k \mathbf{H}) P_k^- \quad (4.13)$$

Finally, we repeat the prediction and update steps until the desired time finished.

4.3 The Simulation Results

IMU measurements were conducted with 10 Hz, and its variances (from Table 4.1) are 1.734×10^{-4} in the x-direction and 1.386×10^{-4} in the y-direction. DVL using low update rate around 2Hz and its variances are 4.462×10^{-4} in the x-direction and 4.581×10^{-4} in the y-direction. SBL has a low and unstable update rate. In this case, we generated an update rate randomly between [0.5 - 1] Hz for SBL and to match it with other sensor measurements, some of the measurements have been duplicated randomly.

That indicates no new measurements for the duplicated measurements. A white Gaussian noise has been added to the measurement trajectories to simulate the real measurements. The simulation shows the true trajectory, measurement trajectory, and KF trajectory. For the true measurements, Table 4.2 presents the values of the true trajectory for a sine wave.

Table 4.2 The true measurements as a sine wave for the simulation.

Positions in X, Y direction	Velocities in X, Y direction	Accelerations in X, Y dir.
$P_{x,True} = t$ (m)	$v_{x,True} = 1$ (m/s)	$a_{x,True} = 0$ (m/s ²)
$P_{y,True} = \sin(t)$ (m)	$v_{y,True} = \cos(t)$ (m/s)	$a_{y,True} = -\sin(t)$ (m/s)

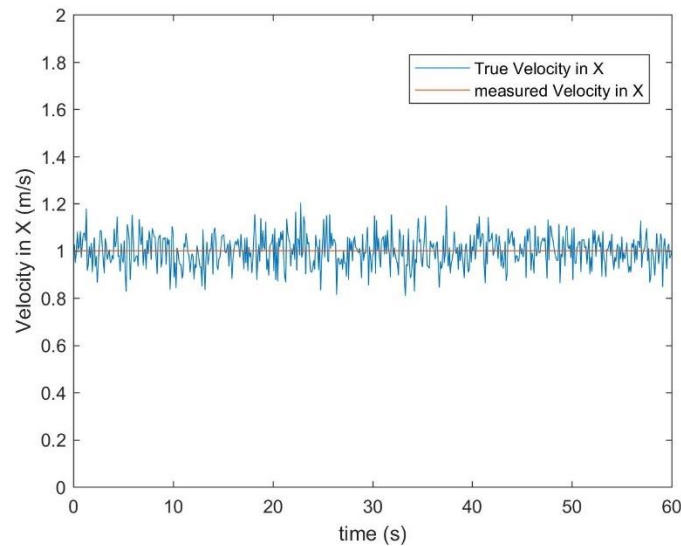


Figure 4.3 The true velocity compares to measured velocity in the X direction.

Where the velocity measurements are defined as follows

$$\text{the velocity measurement} = \text{the "true" velocity} + \text{Noise} \quad (4.14)$$

Where the noise is a white noise that has zero mean and each sensor has different noise values that usually depend on its variance and other factors. Figure 4.3 shows the true velocity compare to measured velocity in the X direction.

In Figure 4.4, the true trajectory is a sine wave, the measurement is from SBL, and the estimated positions were generated from KF by fusing the IMU and SBL measurements.

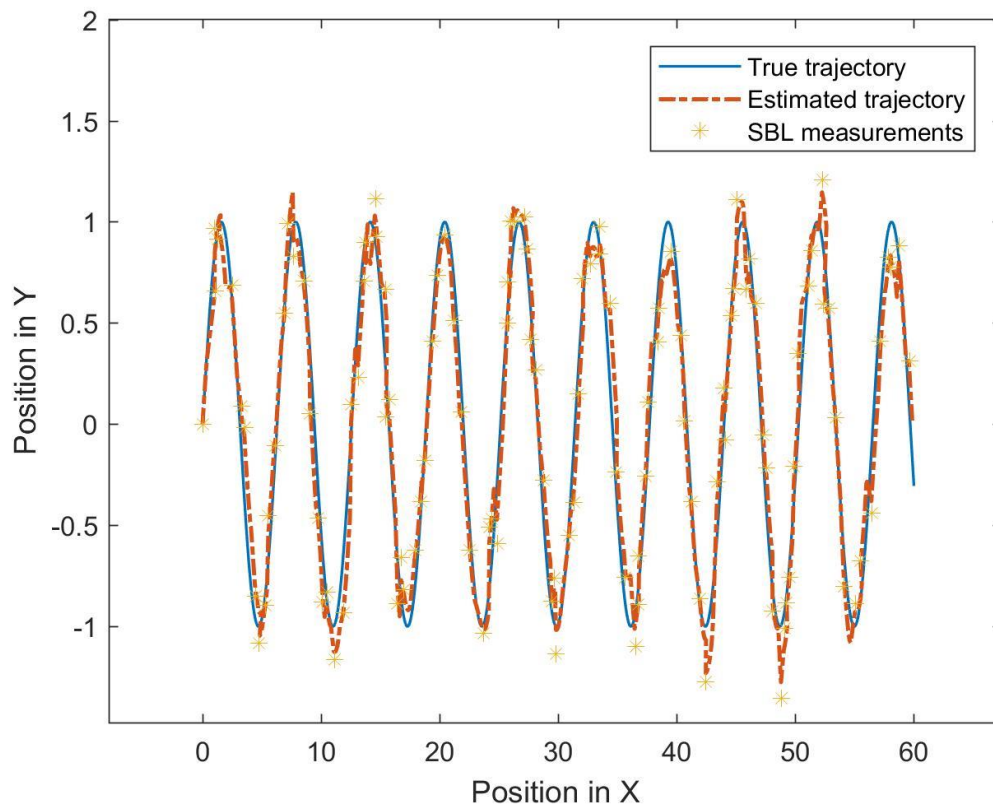


Figure 4.4 The true trajectory as a sine wave, SBL measurements, and the estimated trajectory.

To verify the performance of the filter, the standard deviation of the measurement and the estimation errors were calculated as shown in Figure 4.5.

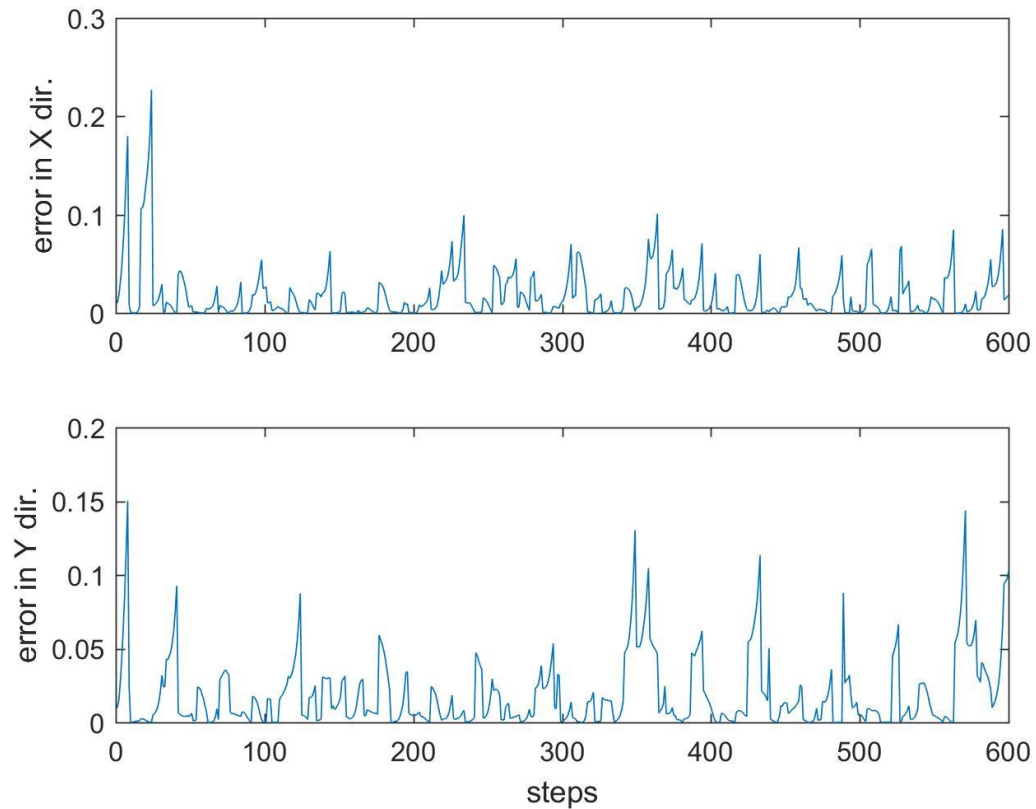


Figure 4.5 The estimation errors in the positions.

In addition, different trajectories were generated to verify the performance. In Figure 4.6, the true trajectory is in a circle path, and Figure 4.7 shows a straight line as a true trajectory.

The true trajectory (the blue path) in Figure 4.6 is shown as a circle with a radius of 1 (m), and the true velocity of the body is 1 (m/s). Also, the yellow stars represent the SBL measurements. Finally, the estimated trajectory is obtained from the fusion of measurements by using KF. In Figure 4.7 the true path is shown as a straight line, and the true velocity of the body is 1 (m/s).

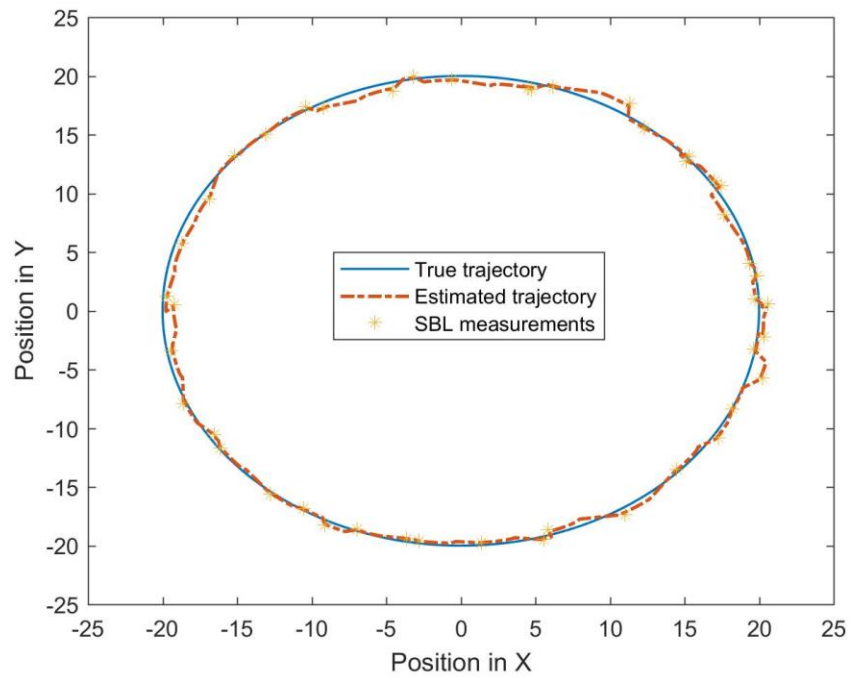


Figure 4.6 The true trajectory as a circle, SBL measurements and the estimated trajectory.

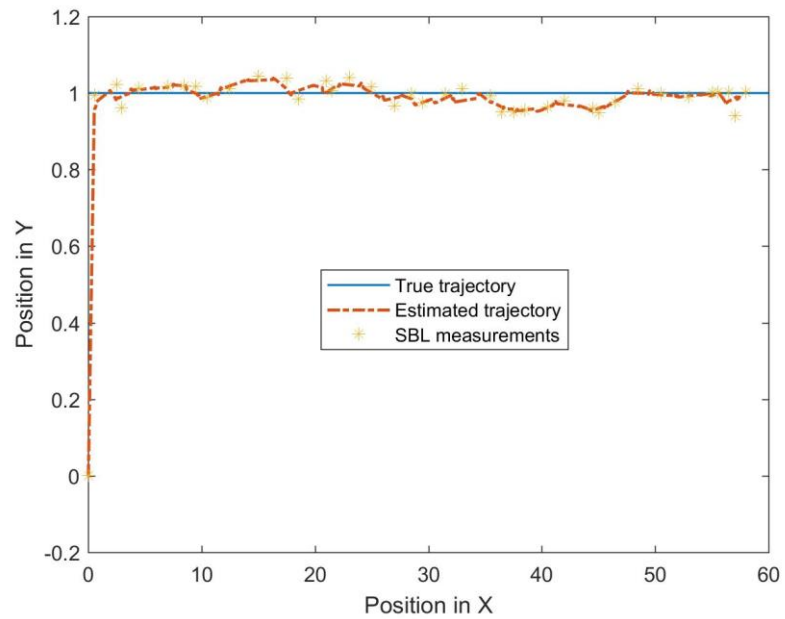


Figure 4.7 The true trajectory shows a straight line, SBL measurements, and the estimated trajectory.

4.4 The Experiments Results

This section talks about the experiment's results, which were carried out by INS/SBL fusion method. The total tests done were seven water tests, and the location was a swimming pool in Embry-Riddle Aeronautical University. Figure 4.8 represents the campus' swimming pool, and the red path is the expected or the "true" path of AUV on the test.

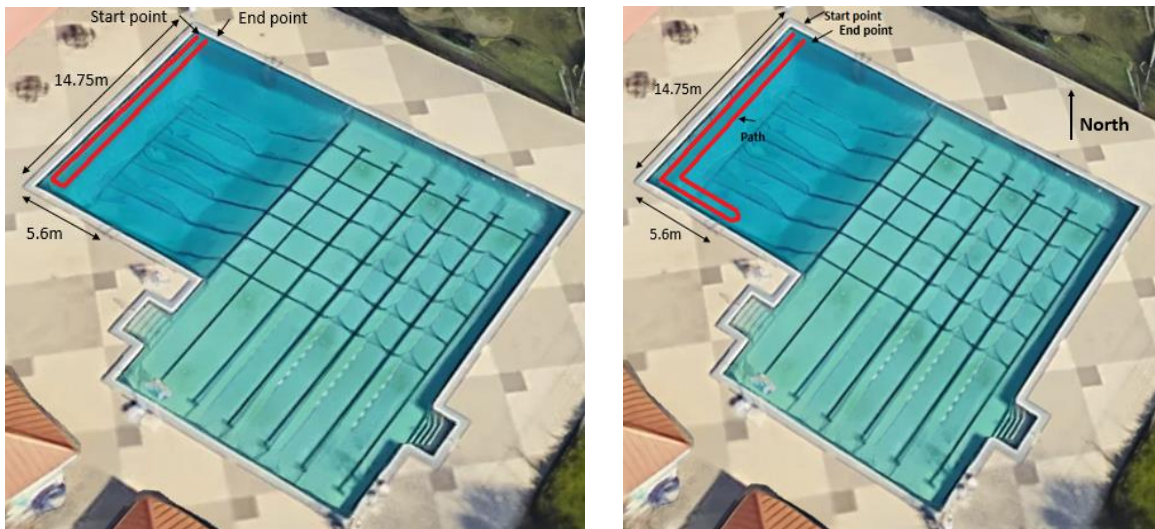


Figure 4.8 The swimming pool of the campus. The red path represents the expected path, and they are the 'forward and backward' path and 'L' path.

The swimming pool of the campus is made in L shape, which is also described in the diagram. The deep area of the swimming pool constructed to the left side and the total length of the edges is approximately 15.76 meters, and the short edges are calculated to be 5.6 meters. The long side swimming pool and its heading is around 220 degree, which was measured with the help of the phone's compass. There were two different groups of tests that were carried out in the swimming pool on different days. The first test

conducted had four tests, and they took place on November 5th, 2017, and the second test was of three tests conducted on November 11th, 2017 that is one week after the first set.

There were two tests conducted on November 5th, as mentioned above. The Yellowfinn II had a task to carry out the forward and backward sort of movements, and they had to be done along the side of the pool which was long in length. When the Yellowfinn II completed the distance to the end of the side which was long, the 180-degree turn was made by the Yellowfinn II, and it returned back to the point from where it started. That was for all the two tests on November 5th, and for the three tests of November 11th, the Yellowfinn II had done a movement in L shape, and its movement was along the side of edges of the swimming pool.

There were three approaches for the experiments:

- 1- Creating an estimated path based on EKF by using only INS.
- 2- Creating an estimated path based on UKF by using only INS.
- 3- Creating an estimated path based on EKF by using INS and SBL.

4.4.1 INS Path Based on EKF

In the implementation of the EKF in the INS navigation approach, the inputs vector is

$$u = [a_x, a_y, a_z, p, q, r]^T \quad (4.15)$$

where

a_x, a_y, a_z : The accelerations of x, y, z axis in the body-fixed frame.

p, q, r : The angular rate of x, y, z axis in the body-fixed frame

The process error covariance matrix Q , which were tuned and fixed, equals to

$$Q = \begin{bmatrix} 0.01 & 0 & 0 & 0 & 0 & 0 & 0 & 0 & 0 \\ 0 & 0.01 & 0 & 0 & 0 & 0 & 0 & 0 & 0 \\ 0 & 0 & 0.01 & 0 & 0 & 0 & 0 & 0 & 0 \\ 0 & 0 & 0 & 0.01 & 0 & 0 & 0 & 0 & 0 \\ 0 & 0 & 0 & 0 & 0.01 & 0 & 0 & 0 & 0 \\ 0 & 0 & 0 & 0 & 0 & 0.01 & 0 & 0 & 0 \\ 0 & 0 & 0 & 0 & 0 & 0 & 0.01 & 0 & 0 \\ 0 & 0 & 0 & 0 & 0 & 0 & 0 & 0.01 & 0 \\ 0 & 0 & 0 & 0 & 0 & 0 & 0 & 0 & 0.01 \end{bmatrix} \quad (4.16)$$

The measurement error covariance matrix R equals to

$$R = \begin{bmatrix} 2.16e-3 & 0 & 0 & 0 & 0 & 0 & 0 & 0 \\ 0 & 4.46e-4 & 0 & 0 & 0 & 0 & 0 & 0 \\ 0 & 0 & 4.58e-4 & 0 & 0 & 0 & 0 & 0 \\ 0 & 0 & 0 & 5.58e-5 & 0 & 0 & 0 & 0 \\ 0 & 0 & 0 & 0 & 6.48e-4 & 0 & 0 & 0 \\ 0 & 0 & 0 & 0 & 0 & 9.36e-5 & 0 & 0 \\ 0 & 0 & 0 & 0 & 0 & 0 & 1.89e-1 & 0 \end{bmatrix} \quad (4.17)$$

The initial value of the covariance matrix P_0 equals to

$$P_0 = \begin{bmatrix} 1 & 0 & 0 & 0 & 0 & 0 & 0 & 0 & 0 \\ 0 & 1 & 0 & 0 & 0 & 0 & 0 & 0 & 0 \\ 0 & 0 & 1 & 0 & 0 & 0 & 0 & 0 & 0 \\ 0 & 0 & 0 & 1 & 0 & 0 & 0 & 0 & 0 \\ 0 & 0 & 0 & 0 & 1 & 0 & 0 & 0 & 0 \\ 0 & 0 & 0 & 0 & 0 & 1 & 0 & 0 & 0 \\ 0 & 0 & 0 & 0 & 0 & 0 & 1 & 0 & 0 \\ 0 & 0 & 0 & 0 & 0 & 0 & 0 & 1 & 0 \\ 0 & 0 & 0 & 0 & 0 & 0 & 0 & 0 & 1 \end{bmatrix}. \quad (4.18)$$

The diagram below explains the different seven paths of the water tests and the calculations had been derived from EKF algorithm and the navigation approach system used was INS. The measurements were taken from inertial sensors in the experiment. The first four tests had been conducted on November 5th, and the last three tests were carried out on November 11th.

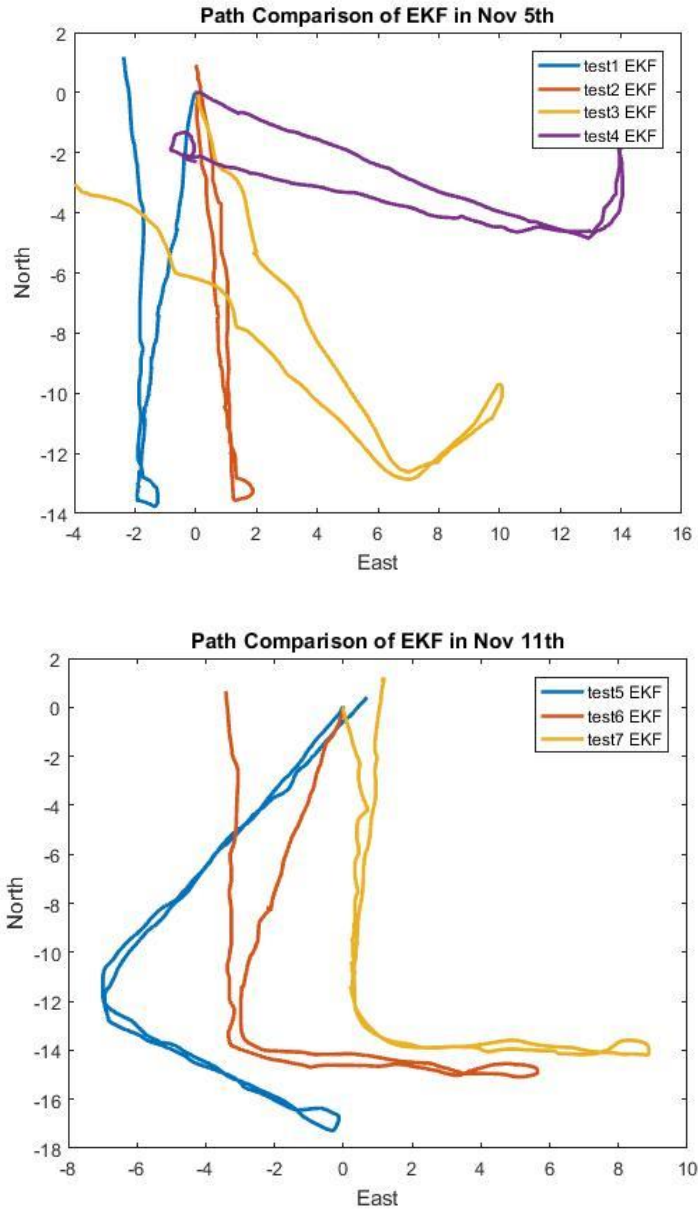


Figure 4.9 All tests' estimated paths based on EKF and only used INS for the navigation.

Figure 4.9 shows the two different paths of the EKF algorithm, and it explains that they are relatively equal to the expected path. The first two tests on November 5th conducted were backward and forward, and the other tests of 3 and 4 were in the L shape movement. The tests carried out in the following were all in the L shape.

The starting headings of all the seven paths were incorrect. The uniform initial heading for all the paths was to be 220 degrees. The gyroscope had some problems with the measurements, and that's why the calculation of yaw angle had an error because it was calculated from the integration of angular rate in the Z direction.

The external measurements were absent from the experiment, and this is the reason the errors could not be removed. Manual measurements of the initial headings for all the tests were the solution to this problem. The expected paths of all tests were already known to us, so the correct initial heading could be measured. The first 10,000 measurements of the yaw angles were calculated, and then the average was taken to find the initial yaw angle of all these tests. These values were shown in Table 4.3.

Table 4.3 The initial yaw angles in all tests.

Test Number	Initial yaw angle
Test 1	-2.9746 rad/ -170.4320 degree
Test 2	2.8565 rad/163.6653 degree
Test 3	2.4548 rad/140.6512 degree
Test 4	2.1185 rad/121.3811 degree
Test 5	-2.6431 rad/-151.4384 degree
Test 6	-2.9022 rad/-166.2838 degree
Test 7	2.9816 rad/170.8330 degree

Table 4.4 provided the difference between the initial yaw angles from IMU and the correct initial yaw angle for all the tests, which is (3.8397 rad / 220 degree or -2.4435 rad/-140 degree).

Table 4.4 The differences between the measured initial yaw angles and correct initial yaw angles.

Test Number	Angle difference
Test 1	0.5235 rad / 30 degree
Test 2	1.0995 rad / 63 degree
Test 3	1.2217 rad / 70 degree
Test 4	1.5708 rad / 90 degree
Test 5	0.2617 rad / 15 degree
Test 6	0.4537 rad / 26 degree
Test 7	0.8726 rad / 50 degree

By using Table 4.4, we can correct the initial yaw angles of all test based on. Figure 4.10 shows the paths of four test after the correction heading.

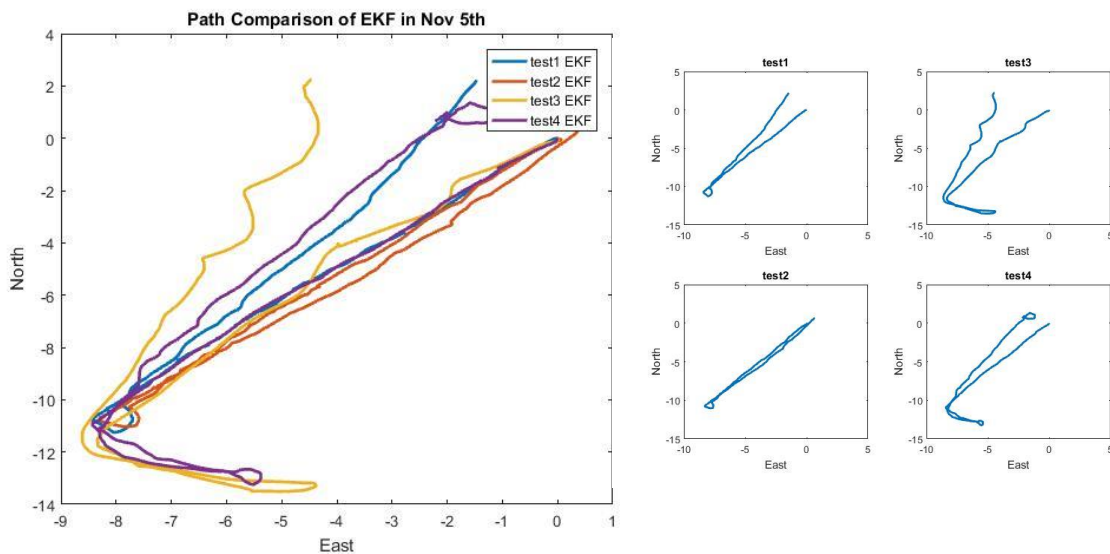


Figure 4.10 Four test on Nov 5th after corrected the heading.

The paths from Figure 4.10 were seen to be overlapping after the rotation was done and that shows Yellowfinn II was traveling along the same side of the swimming

pool. The two points: start and end overlap each other in test 2 and in tests 1, 3 and 4, the starting and the ending points are not the same as shown in Table 4.5.

Table 4.5 Comparison of distances between start points and end points in four tests.

Test Number	The distance between the start point and the end point
Test 1	2.64 meters
Test 2	0.76 meter
Test 3	4.98 meters
Test 4	2.31 meters

In theory, the starting and the ending points should be the same for all the four tests conducted. However, there were accumulated errors in the different estimates, and thus the start and end points could not be the same for all the tests. The test 3 showed that the accumulated error was the largest, and it was 4.98 meters and the minimum error was in test 2 which was 0.76 meters.

Table 4.6 compares the swimming pool's real length with the length of test 1 and 2. The error found between these two lengths were 0.27 meter for the first test and 0.66 meters for the second test.

Table 4.6 Comparison of the estimated lengths with the swimming pool length.

	Swimming pool long side edge
True length of the swimming pool	15.76 meters
Estimation from test 1	15.49 meters
Estimation from test 2	15.11 meters

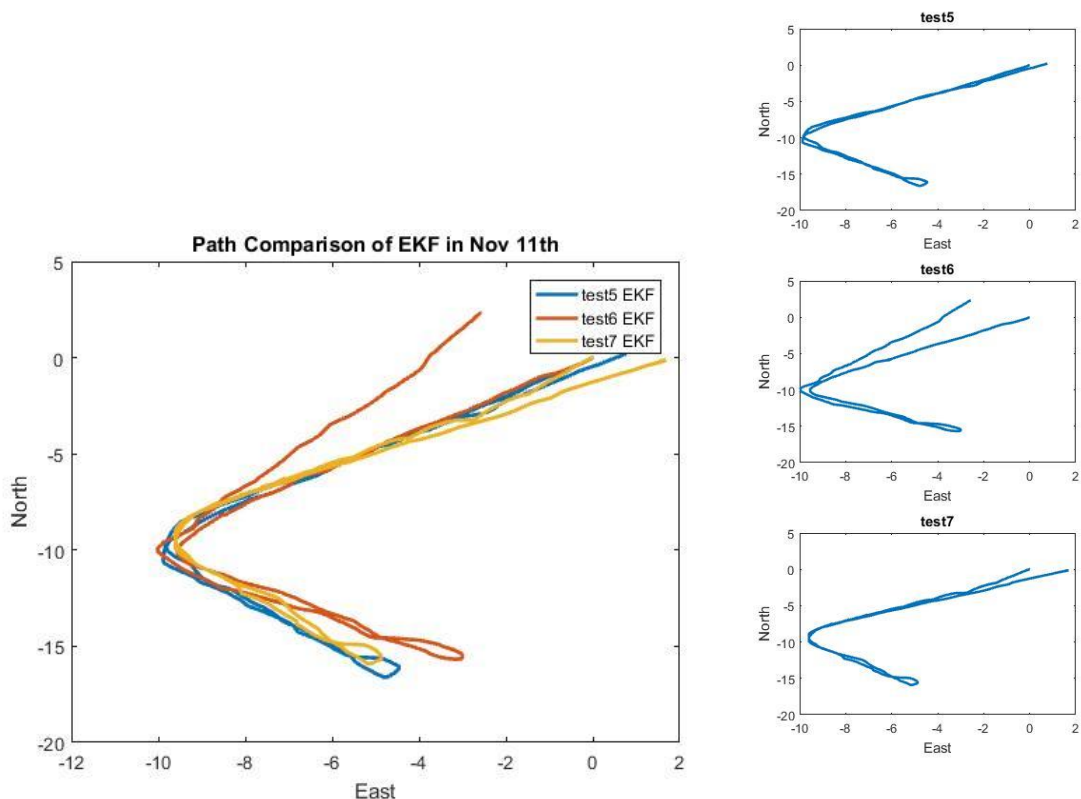


Figure 4.11 The Nov 11th tests after correcting the heading.

When the rotation was done with the second group of tests, it was seen that different paths from the second group were overlapping each other and that was seen in the first test as well. The second group had all the tests in the L movement, and thus the length of the swimming pool could not be calculated around the edges. However, we can still compare the difference between the start point and end point in these tests 5,6, and 7.

Table 4.7 Comparison of distances between start points and end points in the three tests.

Test #	The distance between the start point and the end point
Test 5	0.91 meter
Test 6	3.44 meters
Test 7	1.62 meters

The difference between the starting and the ending points was minimum in test 5 from Table 4.7. The difference was 0.91 meters. Also, the largest difference was found in test 6, which was 3.44 meters. The estimations data was integrated from the measured data, and that's why all the estimations have unbounded errors.

4.4.2 INS Path Base on the UKF

This section will explain the estimated paths which are created by using UKF for the seven water tests, and the measurements were collected from INS only. In the algorithm of UKF, there is a similarity with the EKF algorithm which was the process model and the observations or the measurements model. The same matrices were seen in EKF algorithm were used for UKF, which are the measurement error covariance matrix and the process error covariance matrix. Moreover, we used the same initial values for the state's vector. Figure 4.12 shows paths of seven water tests that based on the UKF algorithm.

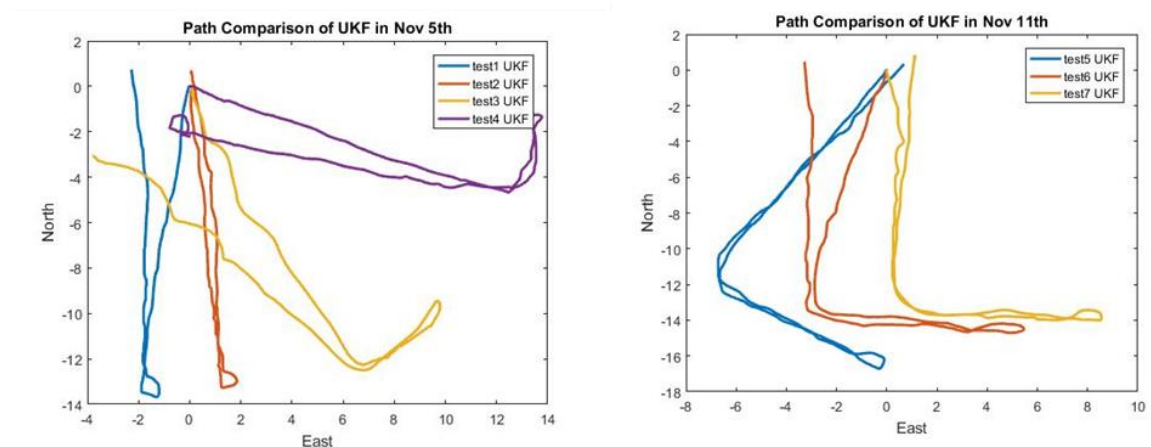


Figure 4.12 The estimated Paths of the seven tests that were created by using UKF.

The Figure 4.12, here we have the same issue in the initial headings with the EKF's paths. The initial headings of each part are incorrect, so a modification should be

done. Since we knew the true heading and we did the calculations in Table 4.4, we can rotate all paths to the correct heading.

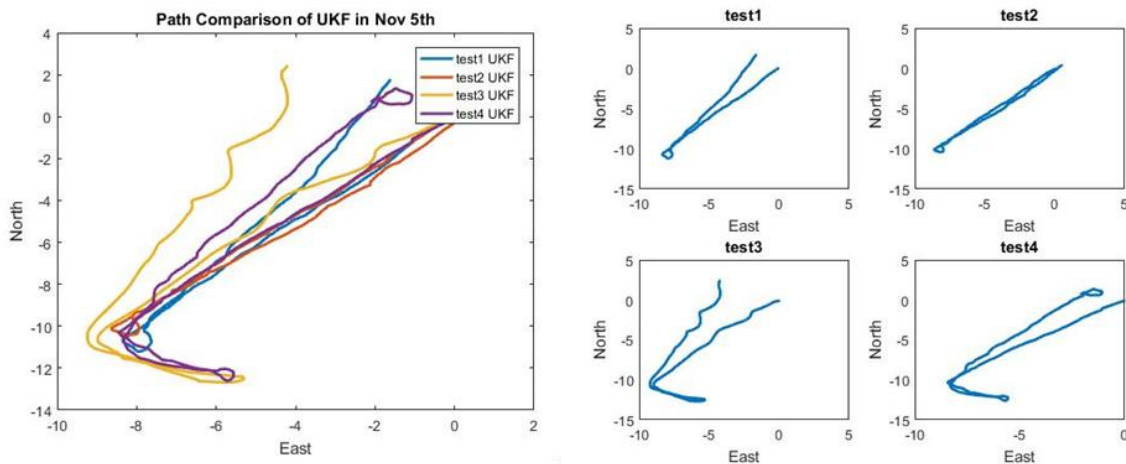


Figure 4.13 The Nov 5th tests after correcting the heading.

The four different paths from 1 to 4 still overlap each other even when they are rotated. Table 4.8 compares the swimming pool’s real length with the length of test 1 and 2 as we did with the previous approach.

Table 4.8 Comparison of the estimated lengths with the swimming pool length.

	Swimming pool long side edge
Real value	15.76 meters
Estimation from test 1	14.65 meters
Estimation from test 2	14.39 meters

Table 4.8 shows the two different estimations and the lengths of test 1 and 2, and they can be seen real close to the original length, and there are slight differences between the real value and the estimated values which are 1.11 m and 1.37 m respectively for tests 1 and 2. The Paths of the second group of water tests after rotations are shown in the Figure 4.14.

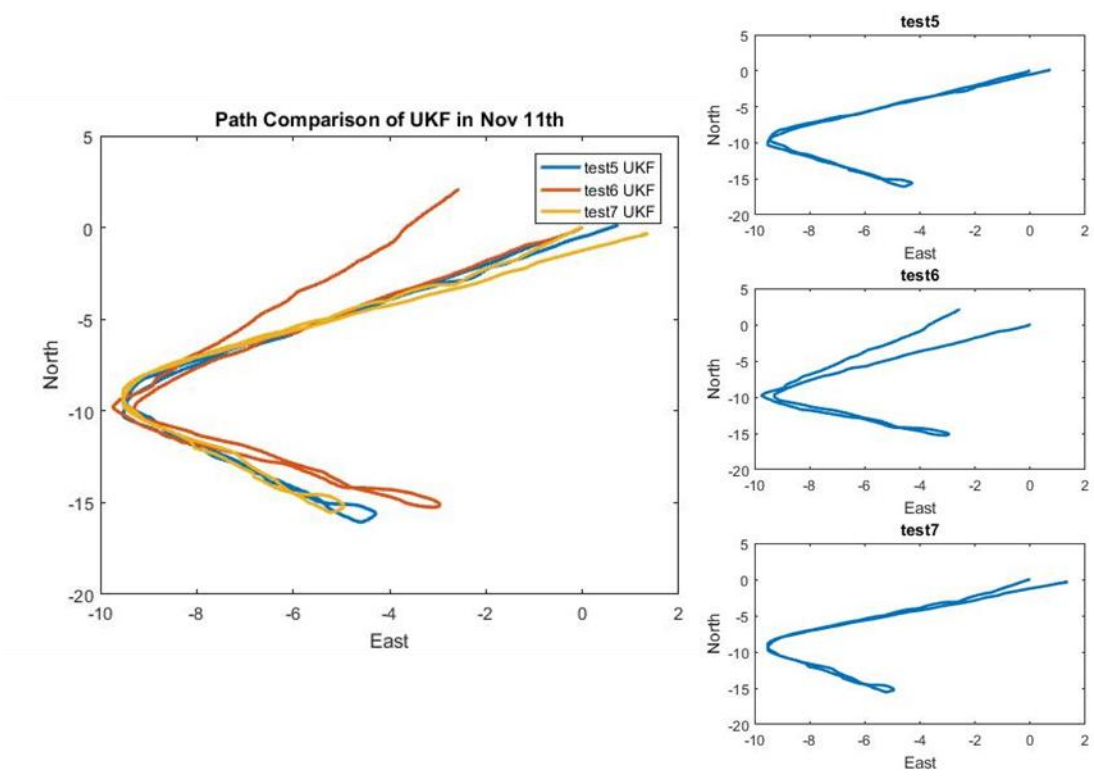


Figure 4.14 The Nov 11th tests after correcting the heading.

All the paths have starting points and ending points and the starting points do not overlap with the endpoints. The differences between these two paths are calculated in Table 4.9.

Table 4.9 Comparison of distances between start points and end points in the three tests of Nov 11th tests.

Test Number	The distance between the start point and the end point
Test 5	0.75 meter
Test 6	3.28 meters
Test 7	1.36 meters

The above Table 4.9 shows the differences between the starting points and the ending points for the three tests which are 0.75 m, 3.28 m and 1.36 m respectively.

4.4.3 Compare the Paths from The EKF and UKF

This section will compare the results of EKF algorithm in comparison to UKF algorithm. In both approaches, the INS navigation only was used. The first comparison is the estimated paths of November 5th.

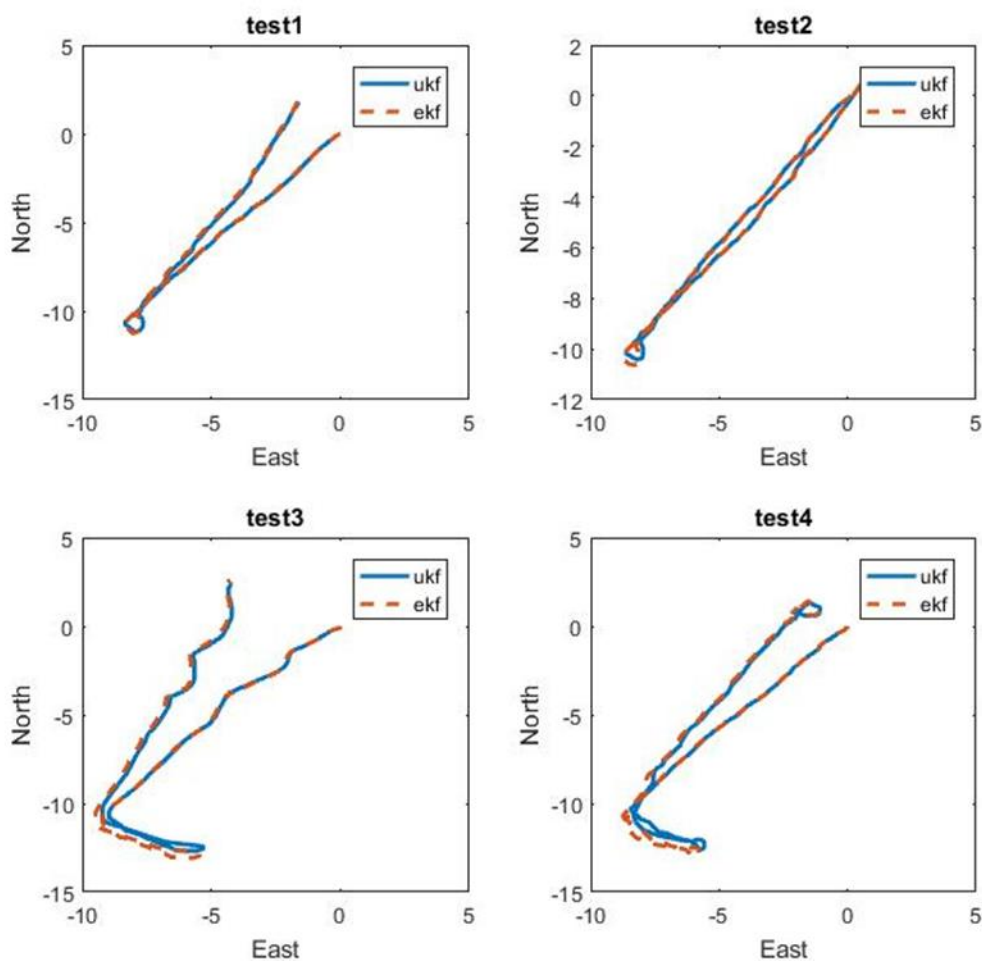


Figure 4.15 Comparison of UKF and EKF paths for tests Nov 5th.

The performance of EKF and UKF are compared, and Table 4.10 is comparing the starting with the ending points of each test. These results illustrate that the UKF algorithm has less error than the EKF algorithm.

Table 4.10 Comparison of UKF and EKF in terms of distances between start points and end points.

Test Number	The distance between the start point and the end point in the EKF	The distance between the start point and the end point in the UKF
Test 1	2.64 meters	2.38 meters
Test 2	0.76 meter	0.54 meter
Test 3	4.98 meters	4.83 meters
Test 4	2.31 meters	2.21 meters

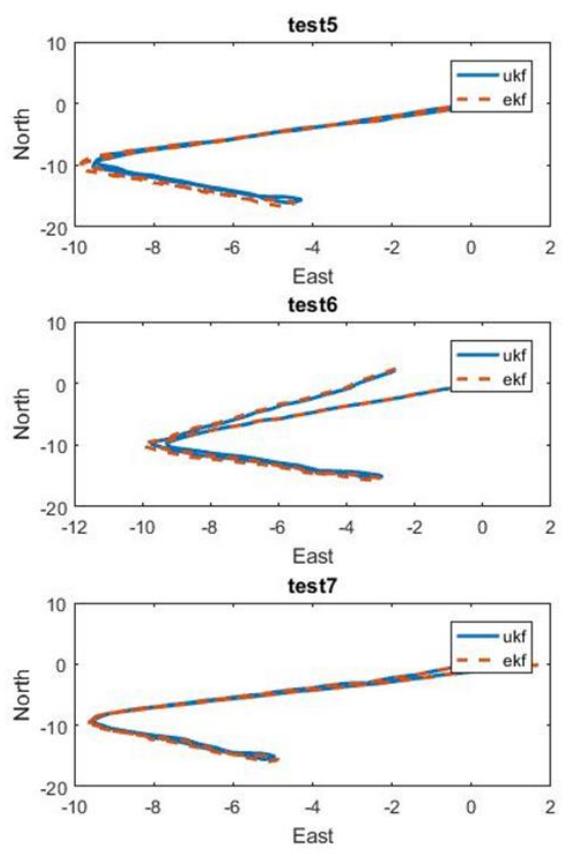


Figure 4.16 Comparison of UKF and EKF paths for tests Nov 11th.

Table 4.11 Comparison of UKF and EKF in terms of distances between start points and end points.

Test Number	The distance between the start point and the end point in the EKF	The distance between the start point and the end point in the UKF
Test 5	0.91 meter	0.75 meter
Test 6	3.44 meters	3.28 meters
Test 7	1.62 meters	1.36 meters

Therefore, a conclusion can be derived from Tables 4.10 and 4.11, which are the errors in UKF are less than the errors in the EKF. The reason for this difference is that the UKF's algorithm does not have to go through the process of linearizing the nonlinear models and thus it means that no information gets lost during this process. The propagation of error by UKF algorithm is another reason why the accurate estimations are met in the end.

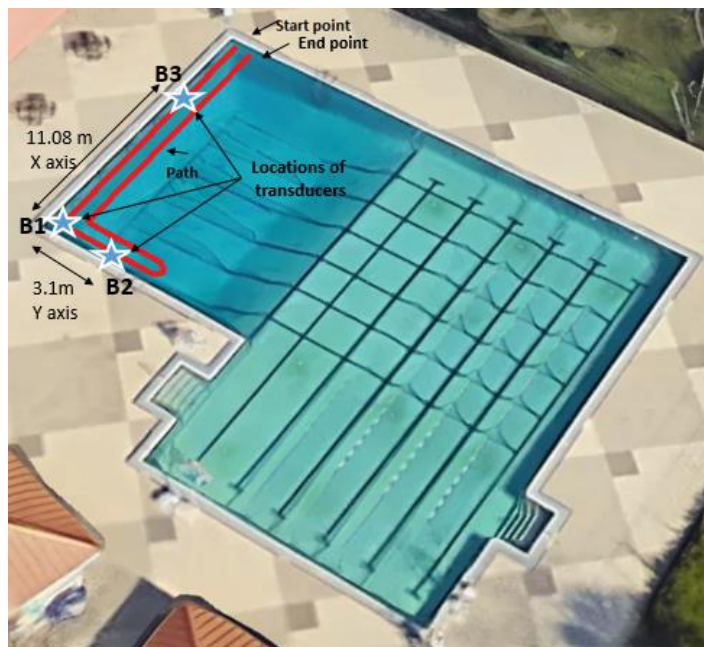


Figure 4.17 The locations of three transducers.

4.4.4 INS/SBL Fusion Navigation Approach Based on EKF

This section will present the different paths of SBL acoustic positioning system and the INS/SBL approach of fusion navigation. There were different transducers installed in the swimming pool before the use of SBL acoustic positioning system. The locations of these transducers were shown in Figure 4.17.

The surface station of SBL is usually connected to three different sonar transducers. These three transducers are named as B1, B2, and B3. The difference between B1 and B2 is 3.1 meters, and the distance between B1 and B3 is 11.08 meters. The transducers are used as the local frame of reference for the navigation of AUV. The local reference is identified initially at sonar B1 and its axis to the Sonar B3 as the X-axis. The Y-axis is taken as Sonar B1 to Sonar B2. The coordinates for the three transducers in the local reference frame are shown as (0,0), (0,3.1) and (11.08,0) respectively.

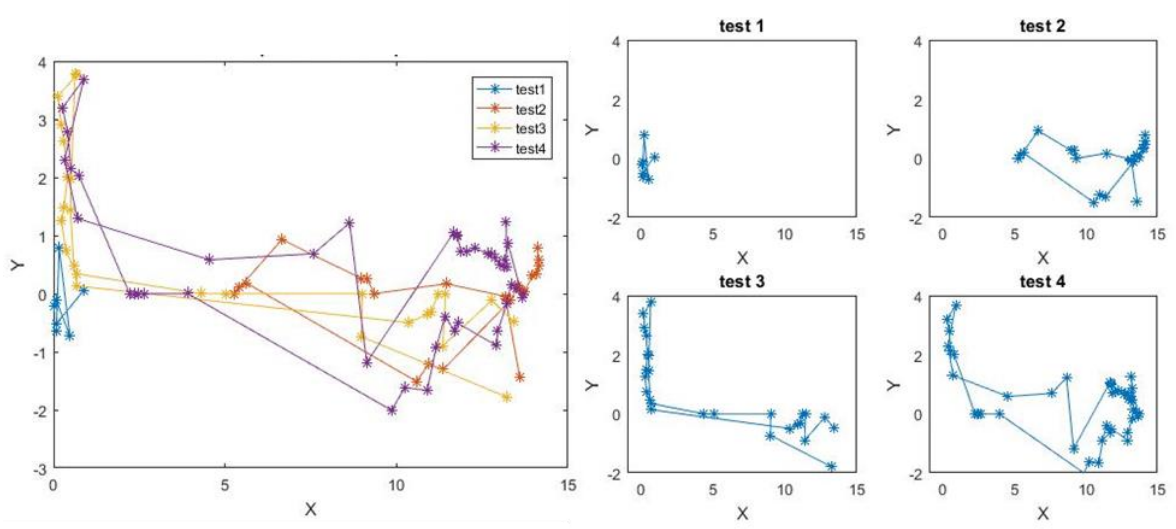


Figure 4.18 The paths of tests 1-4 were from the SBL acoustic positioning system in the local reference frame.

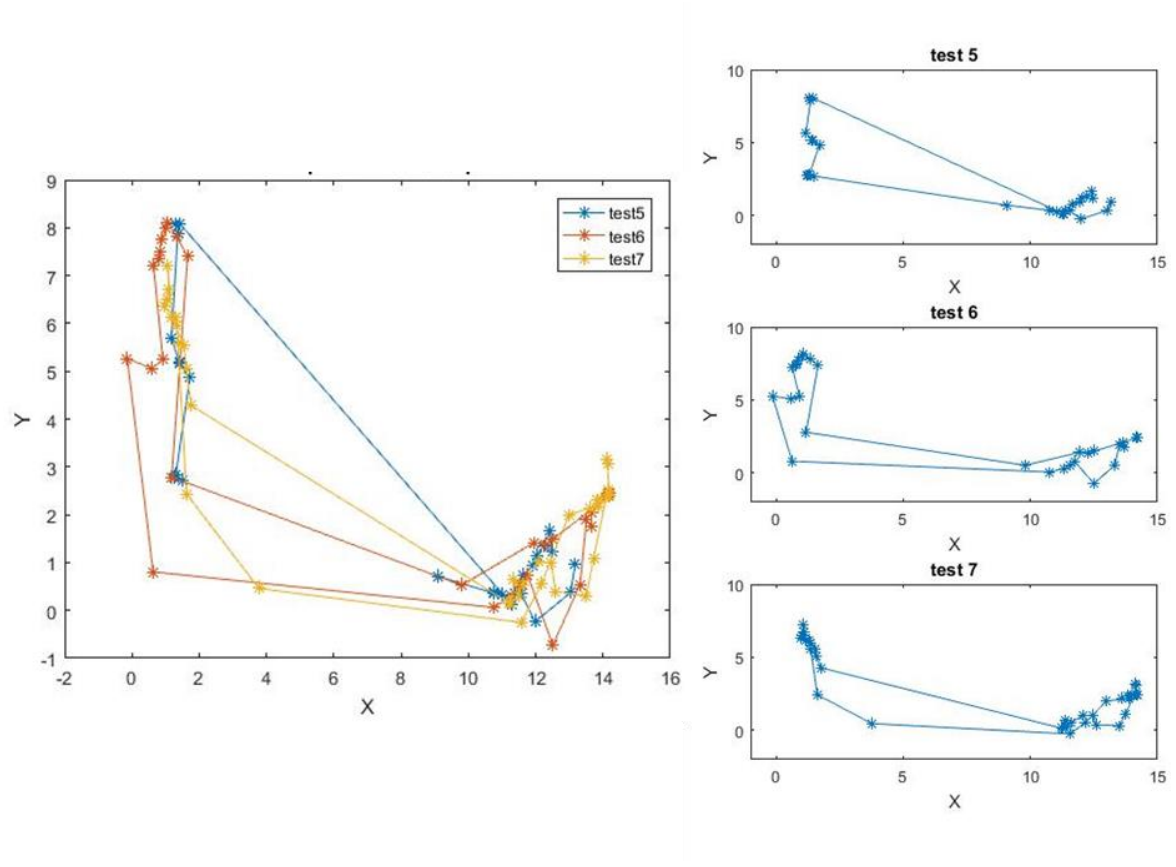


Figure 4.19 The paths of tests 5,6, and 7 were from the SBL acoustic positioning system in the local reference frame.

The Figures 4.18 and 4.19 show the different paths recorded from the SBL acoustic positioning system. The updating rate of SBL is unstable. The time difference is huge for an update because sometimes the system updates in less than 2 seconds and sometimes it takes more than a minute.

There are some reasons behind that unclear measurements. Firstly, the objects in the water often reflect the sonar energy. The ‘B1’ was placed at the very corner of the experimented swimming pool, and the reflection of sonar energy was caused by the walls, and thus the performance of B1 was affected. We needed to place the transducers

below 2 meters in the water; this is the requirement of the pilot SBL system manufacturer. In addition, the two transducers have to be put at least 10 meters apart. Thus, that corner of the pool was the only location left for B1.

There were different noises as well under the swimming pool such as natural and human-made. Hence, transducers needed to hear each other. This means that the signals need to be louder than the noise in the back so that the voice can be heard easily [41]. In reality, there was natural noise in the swimming pool, but there had been the noise of people in the pool and the music which was being played in the background. Thus, it affected the performance of SBL as well of the experiment.

The stability of transducers was significant because they are the essential means of the measurements. Moreover, the baseline could not be shifted because if it was shifted, the positions might get skewed. The swimming pool does not have a high electric current or the tides, but the buoyancies positions often get changed when there is a strong wind blowing, and it changes the position of the transducers as well.

These results depict that the SBL does not have as many acoustic positions as does the INS. Test 3 was the platform from where the measurements were selected so that the accumulated errors in the real INS could be corrected.

The path of SBL should be transferred to NED frame from the local reference before fusing with INS measurements. The heading was found to be the only difference between these two paths. Therefore, the path could be easily converted from local frame to NED which could be done by rotation. This is shown in Figure 4.20.

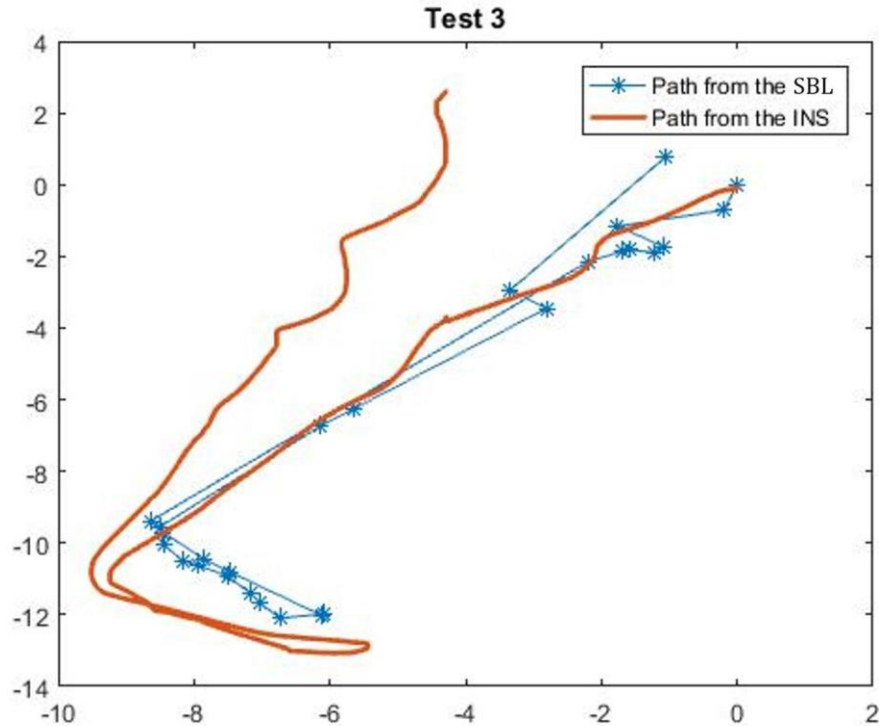


Figure 4.20 Test 3 path from INS and SBL after rotation.

Figure 4.20 shows that the path headings of the SBL and INS are same after rotating the SBL from the local frame to the NED frame. There is a drift problem in INS, and this is the reason the starting and ending points had a difference. Also, if we compare these differences with SBL, they are found to be small in SBL. A more accurate path could be calculated by fusing the SBL data with INS data with the help of EKF algorithm.

The navigation approach of SBL/INS had the EKF algorithm, and the measurements vector had risen from 7 to 9 states. Nevertheless, the measurements error covariance matrix \mathbf{R} needed to be updated. Furthermore, the pilot SBL acoustic approach has a variance on the measurements and thus information could be added to the measurements error covariance matrix. Therefore, the measurements matrix is updated to

$$h = [X, Y, Z, u, v, w, \phi, \theta, \psi]^T \quad (4.19)$$

Moreover, the measurements error covariance matrix is

$$R = \begin{bmatrix} X_{error}^2 & 0 & 0 & 0 & 0 & 0 & 0 & 0 & 0 & 0 \\ 0 & Y_{error}^2 & 0 & 0 & 0 & 0 & 0 & 0 & 0 & 0 \\ 0 & 0 & 2.16e-3 & 0 & 0 & 0 & 0 & 0 & 0 & 0 \\ 0 & 0 & 0 & 4.46e-4 & 0 & 0 & 0 & 0 & 0 & 0 \\ 0 & 0 & 0 & 0 & 4.58e-4 & 0 & 0 & 0 & 0 & 0 \\ 0 & 0 & 0 & 0 & 0 & 5.58e-5 & 0 & 0 & 0 & 0 \\ 0 & 0 & 0 & 0 & 0 & 0 & 6.48e-4 & 0 & 0 & 0 \\ 0 & 0 & 0 & 0 & 0 & 0 & 0 & 9.36e-5 & 0 & 0 \\ 0 & 0 & 0 & 0 & 0 & 0 & 0 & 0 & 0 & 0.189 \end{bmatrix}$$

Notice that in the above equation, X and Y are positions of the AUV in the NED frame, and they are measurements from the SBL acoustic positioning system. Now, we can use the updated EKF's algorithm to fuse measurements, and the fused path is as shown in Figure 4.21. Moreover, Figure 4.22 shows the true trajectory.

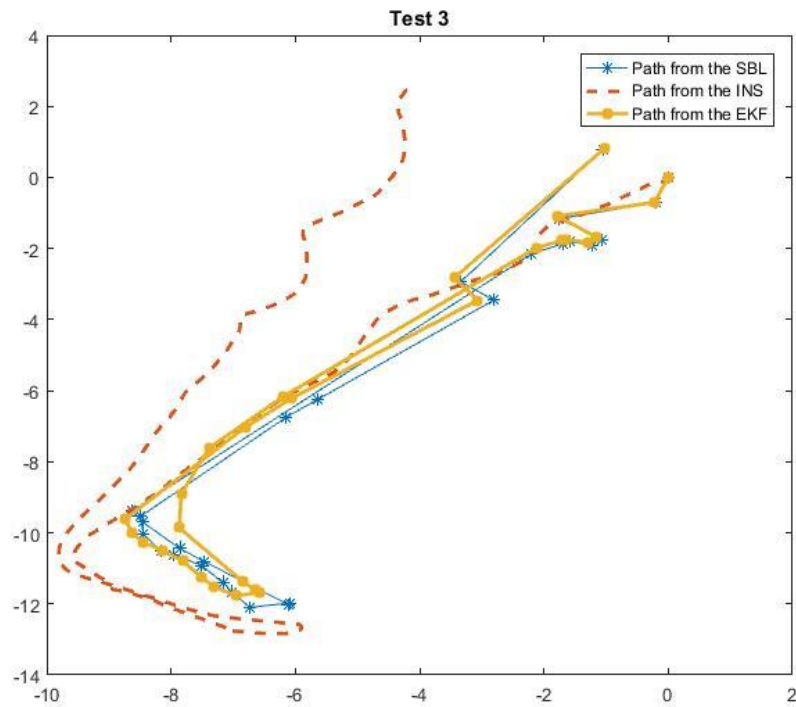


Figure 4.21 Paths from the SBL, INS and SBL/INS based on EKF.

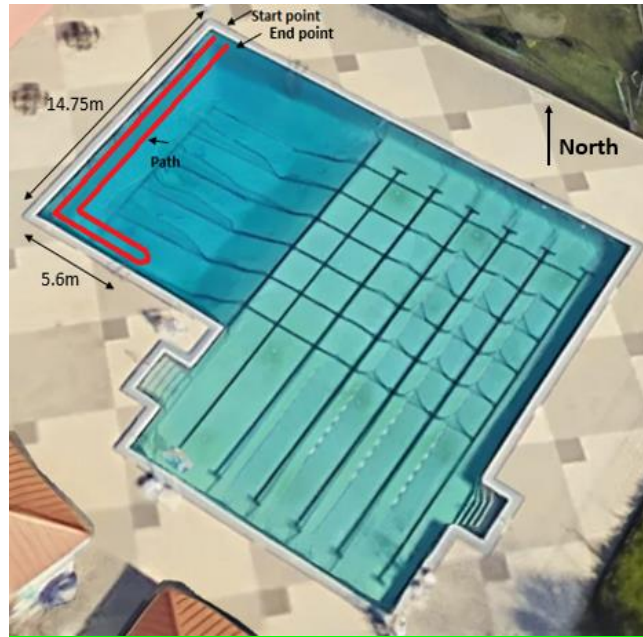


Figure 4.22 The true trajectory of test 3.

The update rate of the fusion navigation approach is equal to the minimum update rate, which is the update rate for the SBL acoustic positioning system. Figure 4.21 illustrates that the INS/SBL fusion navigation approach reduced the accumulated errors on the other approaches. However, the fused path seemed to be closer to SBL path than the INS path. This occurred because the EKF trusts the SBL measurements more than INS measurements, and this is due to the first two values in the diagonal of the measurement error covariance ' \mathbf{R} ' are very small.

Chapter V

Discussion and Conclusions

The primary purpose of this thesis is to study the performance of several methods to perform underwater vehicle's navigation. Various navigation methods were studied and evaluated; those methods include the INS, the SBL acoustic positioning system, and the INS/SBL fusion navigation approach. After conducting several experiments and simulations, we can discuss some of the conclusions.

5.1 Discussion

5.1.1 The INS navigation method

The INS in Yellowfinn II has inertial sensors such as the IMU and the DVL. Two Kalman filter algorithms are used to fuse the measurements from these two sensors which are the EKF and the UKF. The EKF and UKF algorithms are valid, and results are proved from the results of the experiments. Roughly, the estimation of these paths from the two algorithms is inclined to the expected paths. The paths in test 1 and test 2, which were estimated from either EKF or UFK, are accurately matched the length of the swimming pool's edge. This shows that the INS navigation approach is acceptable for a short-range navigation mission.

5.1.2 The performance of EKF and UKF

The UKF's performance is better than the EKF's performance. Theoretically, the nonlinear model of the EKF's algorithm is expanded based on the Taylor series, and the EKF ignores high order terms in the development of the linear model. Therefore, there will be errors in EFK's output when some information is lost on the model. Based on experimental results, the errors in the UKF are slightly smaller than the errors in the EKF.

5.1.3 INS/SBL navigation approach

The fusion of the INS and SBL navigation approach was able to correct the drift problems in the INS. Unbound errors growing in integrations is one of the major drawbacks of the INS which will be added to the estimated position and reflect on the calculated path. The experiments results showed both filters could not remove the accumulated errors in paths when only using INS. The 4.98 meters error for EKF and 4.83 meters error for UKF in test 3 recorded the highest error among the seven-water test, and also lowest error occurred in 0.76 meters for the EKF and 0.54 meter for UKF.

The proposal in this thesis is the fusion INS/SBL navigation approach that uses measurements from SBL acoustic positioning system as external measurements to reduce the unbounded errors in INS. The estimated path based on the fusion INS/SBL navigation approach explicitly in test 3 is close to the true path. Also, in the process of fusion navigation, the unbounded error is being reduced. With this method, only 1.31 meters error detected in the estimated path, but in the initial INS navigation method, the error was 4.98 meters.

Though the positioning of the SBL system is more precise than estimated positions from the INS, the only slight disadvantage is that the SBL acoustic positioning system is not stable for a short-range navigation mission. This error can be detected from data being accumulated from the water tests. Environmental noises and objects in the water contribute immensely to the update rate of the SBL acoustic positioning system. In the long run, we say that the SBL system will give more measurements when there's a long-range navigation mission and broader water environment.

5.2 Conclusions

The navigation and localization for AUVs are particularly challenging due to the unavailability of Global Positioning System (GPS) signals underwater and the complexity of the unstable environment. Alternative methods such as acoustic positioning systems, Inertial Navigation Systems (INS), and the geophysical navigation approach are used for AUV navigation. The significant disadvantage of the INS is the “drift,” the unbounded error growth over time in the outputs. This thesis studied and tested a combined AUV navigation that fuses measurements from the INS and short baseline (SBL) acoustic positioning system to reduce the drift. Several navigation methods were studied and evaluated; those methods include the INS, the SBL acoustic positioning system, and the INS/SBL fusion navigation approach. After conducting the experiments and simulation, we illustrated that using only INS navigation approach is acceptable for a short-range navigation mission. Moreover, UKF showed a better performance than the EKF in the INS. Finally, the INS/SBL fusion navigation approach was able to reduce the drift problems in the INS. Also, it showed more accuracy in the estimations than other approaches especially on a long-range navigation mission, but not suitable for short range mission.

References

- [1] U. H. Perlman, "How much water is there on Earth," [Online]. Available: <https://water.usgs.gov/edu/earthhowmuch.html>.
- [2] V. Upadhyay, S. Gupta, A. C. Dubey, M. J. Rao, P. Siddhartha, V. Gupta, S. George, R. Bobba, R. Sirikonda, A. Maloo and V. Idichandy, "Design and motion control of Autonomous Underwater Vehicle, Amogh," *IEEE Underwater Technology (UT)*, pp. 1-9, 2015.
- [3] J. Kennedy, Decoupled Modelling and Controller Design for the Hybrid Autonomous Underwater Vehicle: MACO, University of Victoria, 2002.
- [4] J. Yuh, "Learning control for underwater robotic vehicles," *IEEE Control Systems*, vol. 14, no. 2, pp. 39-46, April 1994.
- [5] R. Wernli, "The present and future capabilities of deep ROVs," *Marine Technology Society Journal*, vol. 33, no. 4, pp. 26-40, 1999.
- [6] ""What is an ROV"," 22 March 2017. [Online]. Available: http://www.rov.org/rov_overview.cfm.
- [7] ""BlueROV"," [Online]. Available: <http://www.bluerobotics.com/store/rov/bluerov2/>. [Accessed April 2017].
- [8] ""Autonomous Underwater Vehicles"," [Online]. Available: <https://www.nauticalcharts.noaa.gov/csdl/AUV.html>. [Accessed 22 March 2017].
- [9] L. Stutters, H. Liu, C. Tiltman and D. J. Brown, "Navigation Technologies for Autonomous Underwater Vehicles," *IEEE Transactions on Systems, Man, and Cybernetics, Part C (Applications and Reviews)*, vol. 38, no. 4, pp. 581-589, July 2008.
- [10] ""Bluefin Robotics"," [Online]. Available: <http://www.bluefinrobotics.com/about/about-bluefin/>. [Accessed March 2017].
- [11] H. Yan and M. Pearson, "Underwater search resumes for missing Malaysia Airlines plane," 18 April 2014. [Online]. Available: <http://www.cnn.com/2014/04/15/world/asia/malaysia-airlines-plane/>.
- [12] J. Yuh, "Design and Control of Autonomous Underwater Robots: A Survey," *Autonomous Robots*, vol. 8, no. 1, pp. 7-24, 2000.
- [13] R. W. Button, J. Kamp, T. B. Curtin and J. Dryden, A Survey of Missions for Unmanned Undersea Vehicles, National Defense Research Institute, 2009.
- [14] D. Gettinger, "What You Need to Know About Underwater Drones," 16 November 2015. [Online]. Available: <http://dronecenter.bard.edu/underwater-drones/>.

- [15] ""Iver2-580-S", 20 April 2017. [Online]. Available: <http://www.iver-auv.com/iver2580s.html>.
- [16] G. G. Acosta, H. Curti, O. C. Ibáñez and S. Rossi, "Some Issues on the Design of a Low-Cost Autonomous Underwater Vehicle with an Intelligent Dynamic Mission Planner for Pipeline and Cable Tracking," *Underwater Vehicles. InTech.*, 2009.
- [17] J. A. Catipovic, "Performance limitations in underwater acoustic telemetry," *IEEE Journal of Oceanic Engineering*, vol. 15, no. 3, pp. 205-216, July 1990.
- [18] L. Paull, S. Saeedi, M. Seto and H. Li, "AUV Navigation and Localization: A Review," *IEEE Journal of Oceanic Engineering*, vol. 39, no. 1, pp. 131-149, January 2014.
- [19] P. A. Miller, J. A. Farrell, Y. Zhao and V. Djapic, "Autonomous Underwater Vehicle Navigation," *IEEE Journal of Oceanic Engineering*, vol. 35, no. 3, pp. 663-678, July 2010.
- [20] M. Drtil, "Electronics and Sensor Design of an Autonomous Underwater Vehicle," *University of Applied Sciences Koblenz*, 2006.
- [21] A. Bahr, Cooperative Localization for Autonomous Underwater Vehicles, Massachusetts Institute of Technology, 2008.
- [22] L. Wang, "Autonomous Underwater Vehicle Navigation Based On Short Baseline Acoustic Positioning System And Inertial Navigation," Embry-Riddle Aeronautical University, Daytona Beach, 2017.
- [23] T. Fossen, Guidance and control of Ocean vehicles, John Wiley & sons, 1994.
- [24] T. . I. Fossen, Handbook of Marine Craft Hydrodynamics and Motion Control, First ed., John Wiley & Sons Ltd, 2011.
- [25] R. Panish and M. Taylor, "Achieving High Navigation Accuracy Using Inertial Navigation Systems in Autonomous Underwater Vehicles," in *OCEANS, 2011 IEEE - Spain*, Santander, Spain, 2011.
- [26] M. F. Fallon, G. Papadopoulos, J. J. Leonard and N. M. Patrikalakis, "Cooperative AUV Navigation using a Single Maneuvering Surface Craft," *The International Journal of Robotics Research*, vol. 29, no. 12, pp. 1461-1474, 2010.
- [27] H. Durrant-Whyte and T. Bailey, "Simultaneous localization and mapping: part I," *IEEE Robotics & Automation Magazine*, vol. 13, no. 2, pp. 99-110, June 2006.
- [28] J. Salvi, Y. Petillot and E. Batlle, "Visual SLAM for 3D Large-Scale Seabed Acquisition Employing Underwater Vehicles," *IEEE/RSJ International Conference on Intelligent Robots and Systems*, pp. 1011-1016, 2008.

- [29] R. M. Eustice, O. Pizarro and H. Singh, "Visually augmented navigation for autonomous underwater vehicles," *IEEE Journal of Oceanic Engineering*, vol. 33, no. 2, pp. 103-122, 2008.
- [30] X. Xiang, L. Lapierre, B. Jouvencel, G. Xu and X. Huang, "Cooperative Acoustic Navigation Scheme for Heterogenous Autonomous Underwater Vehicles," in *Underwater Vehicles*, In-Tech, 2009, pp. 525-538.
- [31] K. Vickery, "Acoustic Positioning Systems A Practical Overview Of Current Systems," *Proceedings of the 1998 Workshop on Autonomous Underwater Vehicles*, pp. 5-17, 1998.
- [32] D. Ribas, P. Ridao, A. Mallios and N. Palomeras, "Delayed State Information Filter for USBL-Aided AUV Navigation," in *Robotics and Automation*, Saint Paul, 2012.
- [33] X. Yun, E. R. Bachmann, R. B. McGhee, R. H. Whalen, R. L. Roberts, R. G. Knapp, A. J. Healey and M. J. Zyda, "Testing and Evaluation of an Integrated GPS/INS System for Small AUV Navigation," *IEEE Journal of Oceanic Engineering*, vol. 24, no. 3, pp. 396-404, 1999.
- [34] W. Wang, *Autonomous Control of a Differential Thrust Micro ROV*, University of Waterloo, 2006.
- [35] S. J. Julier and J. K. Uhlman, "A new extension of the kalman filter to nonlinear," *The 11th International Symposium on Aerospace/Defence Sensing, simulation and Controls*, Vols. Multi Sensor Fusion, Tracking and Resource Management II, p. 110-121, jun 1997.
- [36] E. Wan, R. V. DerMerwe and A. T. Nelson, "Dual estimation and the unscented transformation," *Advances in Neural Information Processing Systems*, vol. 12, p. 666-672, 2000.
- [37] P. Rigby, O. Pizarro and S. B. Williams, "Towards Geo-Referenced AUV Navigation Through Fusion of USBL and DVL Measurements," *OCEANS*, pp. 1-6, 2006.
- [38] L. Wang, S. Cronin, R. Goring, Z. Joshwick, K. Ormiston and . E. Williams, "Design and Implementation of an Autonomous Underwater Vehicle: Yellowfinn II," 2017. [Online]. Available: www.robonation.org/sites/default/files/Robosub_Paper.pdf.
- [39] O. J. Woodman, "An Introduction to Inertial Navigation," University of Cambridge, 2007.
- [40] M. S. Grewal, R. L. Weill and A. P. Andrews, *Global Positioning Systems, Inertial Navigation, and Integration*, John Wiley & Sons., 2007.
- [41] Desert Star Systems LLC, PILOT, Precision Underwater Acoustic Positioning System, Operator's Manual, Marina, CA: Desert Star Systems LLC, 2007.

- [42] D. Simon, *Optimal state estimation: Kalman, H infinity, and nonlinear approaches*, Hoboken, New Jersey: John Wiley & Sons, 2006.
- [43] E. Coyle, *Localization & Proprioceptive Sensors [PowerPoint presentation]*, Daytona Beach, Florida, 2016.
- [44] K. György, A. Kelemen and L. Dávid, "Unscented Kalman filters and Particle Filter methods for nonlinear state estimation," in *The 7th International Conference Interdisciplinarity in Engineering*, 2014.